1   Active zone protein SYD-2/Liprin-α acts downstream of LRK-1/LRRK2 to regulate

2   polarized trafficking of synaptic vesicle precursors through clathrin adaptor protein

3   complexes

4

5

6   Sravanthi S P Nadiminti[1], Shirley B Dixit[1], Neena Ratnakaran[1], Sneha Hegde[1], Sierra

7   Swords[2], Barth D Grant[2], Sandhya P Koushika[1][†]

8

9   [1]Department of Biological Sciences, Tata Institute of Fundamental Research, Mumbai,

10   Maharashtra - 400 005, India

11   [2]Department of Molecular Biology and Biochemistry, Rutgers University, Piscataway, NJ

12   08854, USA

13

14   [†]Corresponding author

15   spkoushika@tifr.res.in

16 **Abstract**

17   Synaptic vesicle proteins (SVps) are thought to travel in heterogeneous carriers dependent on

18   the motor UNC-104/KIF1A. In *C. elegans* neurons, we found that some SVps are transported

19   along with lysosomal proteins by the motor UNC-104/KIF1A. LRK-1/LRRK2 and the

20   clathrin adaptor protein complex AP-3 are critical for the separation of lysosomal proteins

21   from SVp transport carriers. In *lrk-1* mutants, both SVp carriers and SVp carriers containing

22   lysosomal proteins are independent of UNC-104, suggesting that LRK-1 plays a key role in

23   ensuring UNC-104-dependent transport of SVps. Additionally, LRK-1 likely acts upstream

24   of the AP-3 complex and regulates the membrane localization of AP-3. The action of AP-3 is

25   necessary for the active zone protein SYD-2/Liprin-α to facilitate the transport of SVp

26   carriers. In the absence of the AP-3 complex, SYD-2/Liprin-α acts with UNC-104 to instead

27   facilitate the transport of SVp carriers containing lysosomal proteins. We further show that

28   the mistrafficking of SVps into the dendrite in *lrk-1* and *apb-3* mutants depends on SYD-2,

29   likely by regulating the recruitment of the AP-1/UNC-101. We propose that SYD-2 acts in

30   concert with both the AP-1 and AP-3 complexes to ensure polarized trafficking of SVps.

31

Introduction

Synaptic vesicles (SVs) found at the pre-synaptic terminal contain membrane-associated

proteins, such as Synaptobrevin-1 (SNB-1), Synaptogyrin-1 (SNG-1), SV2, and RAB-3

(Takamori *et al*., 2006). They are known to have a well-defined composition lacking, for

instance, Golgi-resident enzymes (Salazar *et al*., 2004; Takamori *et al*., 2006; Choudhary *et

al*., 2017). The loss of SV proteins (SVps) has been shown to affect neurotransmission

(Nonet *et al*., 1998; Mahoney, Luo and Nonet, 2006; Brockmann *et al*., 2020; Richmond,

Davis and Jorgensen, 1999; Aravamudan *et al*., 1999) and the progression of

neurodegenerative disorders (Kraemer *et al*., 2003). However, the trafficking routes of SVps

in the cell body remain to be fully elucidated. Although SNB-1 and SNG-1 are present along

with RAB-3 at synapses, only a subset of the SNB-1 and SNG-1 carriers that exit the cell

body includes RAB-3 (Choudhary *et al*., 2017; Maeder, Shen and Hoogenraad, 2014).

Likewise, Synaptophysin and SV2 do not appear to be co-transported by the mammalian SV

motor KIF1A (Okada and Hirokawa, 1999), while Synaptophysin and the Zinc transporter

ZnT3 are likely enriched in different populations of synaptic-like microvesicles (Salazar *et

al*., 2004). Additionally, SVp carriers exiting the cell body are tubular as opposed to those

closer to the synapse, which have a defined smaller diameter (Tsukita and Ishikawa, 1980;

Nakata, Terada and Hirokawa, 1998). Prior studies from mammalian cells and *Drosophila*

suggest that some SVps share trafficking routes with lysosomal proteins (Newell-Litwa *et al*.,

2009; Vukoja *et al*., 2018; Rizalar, Roosen and Haucke, 2021). These findings suggest that

SVps emerge from the cell body in precursor or immature transport carriers that likely have a

heterogeneous composition, sharing trafficking routes with lysosomal proteins.

Several genes have been identified as important in the trafficking of SVps. UNC-16/JIP3-

mediated recruitment of LRK-1/LRRK2 on the Golgi seems to be critical for excluding

57   Golgi-resident enzymes from SVp carriers as well as regulating the size of these carriers

58   (Choudhary *et al*., 2017). The AP-3 complex has been shown to play a key role in separating

59   SVps and lysosomal proteins that initially occupy a common intermediate compartment

60   (Newell-Litwa *et al*., 2009). The biogenesis and maturation of precursor vesicles containing

61   the endolysosomal protein LAMP-1, active zone proteins, and SV proteins are regulated by

62   RAB-2 (Götz *et al*., 2021). UNC-104/KIF1A is the kinesin motor important for SVp

63   transport (Hall and Hedgecock, 1991; Okada and Hirokawa, 1999; Zhao *et al*., 2001; Pack-

64   Chung *et al*., 2007). We previously showed that the SVp carriers formed in the *unc-16*/*jip3*,

65   *lrk-1*/*lrrk2*, and *apb-3* (mutant of the β subunit of the AP-3 complex) mutants of

66   *Caenorhabditis elegans* are not exclusively dependent on UNC-104/KIF1A for their transport

67   (Choudhary *et al*., 2017). However, the link between the maturation of SVp carriers and their

68   ability to recruit the SVp motor remains to be well understood.

69

70   Active zone proteins that mark release sites for SVs at synapses have also been shown to co-

71   transport with some SVps (Bury and Sabo, 2011; Xuan *et al*., 2017; Vukoja *et al*., 2018;

72   Lipton, Maeder and Shen, 2018). Moreover, SVps and some active zone proteins, such as

73   ELKS-1, have been shown to co-transport in lysosomal protein-containing packets called

74   presynaptic lysosome-related vesicles (PLVs). These PLVs are dependent on the small

75   GTPase ARL-8, an interactor of UNC-104/KIF1A/IMAC, which is thought to facilitate

76   UNC-104/KIF1A interaction with the PLVs (Vukoja *et al*., 2018). Additionally, active zone

77   proteins Piccolo and Bassoon present in clusters with Synaptobrevin, Synaptotagmin, and

78   SV2, are thought to be important in forming such transport clusters (Tao-Cheng, 2020).

79   Together, these data suggest that SVp and lysosomal protein trafficking and transport can be

80   regulated by active zone proteins.

81

82   SYD-2/Liprin-α, an active zone protein, is known to interact with and bind to the SV motor

83   UNC-104/KIF1A (Zheng *et al*., 2014; Shin *et al*., 2003; Wagner *et al*., 2009; Stucchi *et al*.,

84   2018). SYD-2/Liprin-α also influences the distribution of acidic organelles such as SVs

85   (Zheng *et al*., 2014), dense core vesicles (Goodwin and Juo, 2013), and lysosomes (Edwards

86   *et al*., 2015b). Active zone proteins SYD-2 and SYD-1 along with synapse assembly proteins

87   SAD-1 and CDK-5 are known to regulate lysosomal protein trafficking in *unc-16* mutants

88   through dynein (Edwards *et al*., 2015b). ELKS-1, which binds SYD-2 (Ko *et al*., 2003; Dai *et*

89   *al*., 2006), has been shown to interact with RAB-6 to regulate the trafficking of melanosomal

90   proteins (Patwardhan *et al*., 2017) and SVs (Nyitrai, Wang and Kaeser, 2020). These studies

91   suggest that SYD-2 can affect the trafficking of SVs and other acidic organelles.

92

93   In this study, we used the *C*. *elegans* touch receptor neuron (TRN) model to better define the

94   co-transport and eventual separation of SV and lysosomal proteins. Importantly, we show

95   that LRK-1 and the AP-3 complex, which we previously identified as important for

96   regulating SV precursor composition (Choudhary *et al*., 2017), play a critical role in sorting

97   lysosomal proteins away from SVps. Furthermore, the active zone protein SYD-2/Liprin-α

98   plays a key role along with UNC-104/KIF1A in the transport of compartments containing

99   both SVps and lysosomal proteins in the absence of the AP-3 complex. Our data suggest that

100   although the SV motor can be recruited on compartments that contain both SVps and

101   lysosomal proteins, SV precursors lacking lysosomal proteins appear to preferentially recruit

102   the SV motor UNC-104.

103

104

105   **Results**

106   **Synaptic vesicle proteins travel with lysosomal proteins in heterogenous carriers**

107   Although studies have indicated that SVps are transported in heterogeneous carriers, the

108   composition of these carriers has not been fully examined. Here, we assessed the co-transport

109   of specific SVps with one another and with other endomembrane compartment proteins in the

110   proximal posterior lateral mechanosensory (PLM) neuron of *C. elegans* (Fig. S1A, S1B-G;

111   Movies S1 and S2).

112

113   Less than 10% of moving RAB-3- and MAN-II-containing vesicles co-transport both markers

114   (Fig. 1A). Likewise, ~10% of SNG-1 and SNB-1 are co-transported with the lysosome-

115   specific cystine transporter, cystinosin (CTNS-1) (Kalatzis *et al*., 2001) (Fig. 1A and Movie

116   S1). Nearly all CTNS-1- and RAB-7-carrying compartments co-transport SNG-1, while only

117   ~50% of CTNS-1-labelled compartments co-transport SNB-1 (Fig. 1B). CTNS-1-labelled

118   compartments move in both the anterograde and retrograde directions in wildtype (Fig. 1C).

119   Approximately 30% of SNG-1 and RAB-7 are co-transported (Fig. 1A, Movie S2).

120   Furthermore, nearly every CTNS-1-carrying compartment co-transports RAB-7, while only

121   ~40% of RAB-7-carrying compartments co-transport CTNS-1 (Fig. 1D). RAB-3, a synaptic

122   vesicle RAB, does not co-transport with CTNS-1, while RAB-3 and RAB-7 are co-

123   transported ~10% of the time (Fig. 1A). RAB-3 is co-transported with SNB-1 and SNG-1

124   approximately 35% of the time (Fig. 1A). Thus, SVp carriers exiting the cell body largely

125   exclude the Golgi-resident enzyme MAN-II and lysosomal proteins.

126

127   To further characterize these compartments that contain both SVps and CTNS-1 or RAB-7,

128   we examined their localization along the PLM process. Unlike SVps in wildtype animals,

129   CTNS-1-labelled compartments are largely restricted to the PLM cell bodies, are present in

130   the first 25 μm of the neuronal process in ~27% of the animals, and never reach the PLM

131   synapse (Fig. 1E, 1F, and S1H). RAB-7-labeled compartments are present in the proximal 25

132   μm of the neuronal process in 52% of the animals but are also absent from the PLM synapse

133   (Fig. 1F and S1I).

134

135   Thus, lysosomal proteins that exit the cell body are present along with some SVps in carriers

136   that we hereafter refer to as the SV-lysosomes or SV-lysosomal compartments. However,

137   only a minority of SNG-1 or SNB-1 travel in CTNS-1-carrying compartments. RAB-3 is

138   excluded from SV-lysosomal compartments and may therefore mark only SV precursors. For

139   this study, we consider the CTNS-1-marked compartments as the SV-lysosomes, since nearly

140   all CTNS-1-carrying compartments also contain SNG-1 (Fig. 1B).

141

142   **LRK-1 and the AP-3 complex exclude lysosomal proteins from SVp transport carriers**

143   Mammalian AP-3 has been shown to play a role in separating lysosomal proteins from SVps

144   (Newell-Litwa *et al*., 2009). As LRK-1 and APB-3 are also known to affect the trafficking of

145   SVps (Choudhary *et al*., 2017), we investigated whether these genes regulate the trafficking

146   of the SV-lysosome compartments in *C. elegans* TRNs.

147

148   There is a small but significant reduction in the co-transport of SNG-1 and RAB-3 in *lrk-1*

149   (~25%), but not in *apb-3* mutants (~40%), which largely resembles the co-transport seen in

150   wildtype TRNs (~35%) (Fig. 2A, Suppl. Table 3, Movies S3 and S4). Interestingly, 45% of

151   SNG-1-carrying vesicles co-transport CTNS-1 in *lrk-1(km17)*, a kinase-deleted loss-of-

152   function mutant. The frequency of SNG-1-carriers containing CTNS-1 is close to 60% in the

153   *lrk-1* null, *lrk-1(km41)*, and *apb-3* mutant animals (Fig. 2B and S2A, Suppl. Table 4). Nearly

154   all CTNS-1-carrying compartments continue to transport SNG-1 (Fig. S2B; Suppl. Table 5).

155   Furthermore, ~80% and ~65% of SNG-1-carrying vesicles co-transport RAB-7 in *lrk-1* and

156   *apb-3* mutants, respectively (Fig. 2C and S2C; Suppl. Table 6, Movie S5). As with CTNS-1,

157   nearly all RAB-7-carrying compartments continue to transport SNG-1 (Fig. S2D; Suppl.

158   Table 7). Notably, the co-transport of CTNS-1 with SNB-1 is not affected in *lrk-1* and *apb-3*

159   mutants (Fig. S2E; Suppl. Table 8), and RAB-3 continues to be absent from CTNS-1-carriers

160   in these mutant animals (Fig. S2F; Suppl. Table 9). Thus, in both *lrk-1* and *apb-3* mutants,

161   the SV-lysosomal compartments show significant transport into the neuronal process,

162   suggesting that both LRK-1 and the AP-3 complex play key roles in sorting CTNS-1 and

163   RAB-7 away from SVps. In these mutants, RAB-3 continues to be excluded from SV-

164   lysosomal compartments and RAB-3 may, therefore, mark the only SVp-containing carriers.

165

166   The localization of lysosomal proteins CTNS-1 and RAB-7 is also altered in both *lrk-1* and

167   *apb-3* mutants. In contrast to wildtype, CTNS-1 is localized to the first 25 μm of the PLM

168   neuronal process in ~63% of *lrk-1* and ~45% of *apb-3* mutants (Fig. 2D, S1H), while 100%

169   of *lrk-1* and ~80% of *apb-3* mutants show RAB-7 up to 25 μm away from the cell body (Fig.

170   2E and S1I). Like CTNS-1 and RAB-7, LMP-1 is largely restricted to the cell body in

171   wildtype animals (Fig. 2F). However, unlike CTNS-1 and RAB-7, LMP-1 localization is only

172   affected in *lrk-1* mutants, with LMP-1 localizing along the neuronal process until the first 50

173   μm in all *lrk-1* animals. In contrast to *lrk-1*, LMP-1 does not localize beyond the first 25 μm

174   of the PLM neuron in *apb-3* mutant animals (Fig. 2F, S1J, and S1K). Since both LMP-1

175   localization and co-transport of SNG-1 and RAB-3 are affected only in *lrk-1* mutants, LRK-1

176   likely affects the trafficking of more kinds of SVp carriers than the AP-3 complex.

177

178   The *lrk-1 apb-3* double mutants, similar to *lrk-1* single mutants, show a significant increase

179   in the co-transport of CTNS-1 and RAB-7 with SNG-1 (Fig. 2B and 2C, Suppl. Tables 4 and

180   6). However, there is an increased number of *lrk-1 apb-3* double mutant animals with CTNS-

181   1 localized along the neuronal process than in either *lrk-1* or *apb-3* single mutants (Fig. 2D

182   and S1H). The *lrk-1 apb-3* double mutants show a similar frequency of animals with RAB-7

183   and LMP-1 localized along the neuronal process as seen in *lrk-1* mutant (Fig. 2E, 2F, S1I,

184   S1J, and S1K). These data suggest that LRK-1 may act upstream of APB-3 in the trafficking

185   of SV-lysosome compartments.

186

187   **LRK-1 regulates localization of the AP-3 complex**

188   LRK-1 acts via the AP-1 and the AP-3 complexes to regulate polarized SVp trafficking and

189   the trafficking of SVp transport carriers. LRK-1 is known to assist in the Golgi membrane

190   localization of the AP-1 clathrin adaptor complex, thereby regulating its function (Choudhary

191   *et al.*, 2017). To examine whether LRK-1 regulates the membrane localization of the AP-3

192   complex as well, we examined the distribution of the β subunit of the AP-3 complex, APB-

193   3::GFP, in neuronal cell bodies of *lrk-1* mutants (Fig. 2G). In wildtype, APB-3::GFP shows

194   punctate localization in the cell body with an average of ~2 to 4 puncta/cell body. In *lrk-1*

195   mutant animals, there are fewer APB-3::GFP puncta per cell body and more cell bodies that

196   lack puncta (Fig. 2G (i) and (ii), 2H and S2G; Suppl. Table 10). The average intensity and

197   size of the APB-3::GFP puncta remain largely unaltered in *lrk-1* mutants (Fig. 2I and 2J;

198   Suppl. Tables 11 and 12). This suggests that, as observed with the AP-1 complex (Choudhary

199   *et al.*, 2017), in *lrk-1* mutants the AP-3 complex may not be recruited efficiently to

200   membrane surfaces. Some of the sorting roles of LRK-1 are likely mediated by facilitating

201   AP-3 localization to membrane surfaces.

202

203   **SV-lysosomes in *lrk-1* and *apb-3* mutants are dependent on UNC-104**

204   SVps are known to be dependent on the anterograde motor UNC-104/KIF1A for their exit

205   from neuronal cell bodies (Hall and Hedgecock, 1991; Pack-Chung *et al*., 2007; Okada and

206   Hirokawa, 1999; Kumar *et al*., 2010). SV-lysosomes likely depend on IMAC/KIF1A in

207   *Drosophila* neurons (Vukoja *et al*., 2018). However, the transport of SVp carriers in *lrk-1* and

208   *apb-3* mutants is only partially dependent on UNC-104 (Choudhary *et al*., 2017). To examine

209   the UNC-104 dependence of the SV-lysosomes, we characterized the role of UNC-104 in

210   transporting both SVs and SV-lysosomes out of neuronal cell bodies using a weak cargo

211   binding-defective hypomorph, *unc-104*(*e1265tb120*) (Kumar *et al*., 2010).

212

213   SNG-1 in *lrk-1* is partially dependent on UNC-104, as little SNG-1 reaches the synapse in

214   *lrk-1*; *unc-104* compared to that in *lrk-1* mutant animals (Fig. 3B). In a strong loss-of-

215   function *unc-104* allele, RAB-3 in *lrk-1* is partially dependent on UNC-104 (Choudhary *et*

216   *al*., 2017). However, with a weak loss-of-function *unc-104* allele, RAB-3 reaches the synapse

217   in *lrk-1*; *unc-104* double mutants (Fig. S3A). SNG-1- and RAB-3-carriers in *apb-3* are

218   partially dependent on UNC-104, as both markers do not reach the synapse in *apb-3; unc-104*

219   double mutants (Fig. 3B and S3A). This suggests that SVps in *lrk-1* and *apb-3* mutants are

220   only partially dependent on UNC-104. Additionally, RAB-3 and SNG-1 in these mutants

221   appear to have slightly different extents of dependence on UNC-104.

222

223   We next examined the CTNS-1-containing SV-lysosomes, which are dependent on UNC-104

224   for their exit from the cell body (Fig. 3C, S3B, S1H). The localization of CTNS-1 is

225   dependent on UNC-104 in *apb-3* mutants but not in *lrk-1* mutants (Fig. 3C and S1H).

226   Compared to *lrk-1* single mutants, there is an increased number of animals with CTNS-1

227   localized along the neuronal process in *lrk-1; unc-104* double mutants (Fig. 3C and S1H).

228

229   The fraction of SNG-1-carrying vesicles co-transporting CTNS-1 is comparable in wildtype,

230   *unc-104*, and *apb-3; unc-104* animals (Fig. 3D; Suppl. Table 13, movie S6). However, in *lrk-*

231   *1; unc-104* mutants, a higher number of SNG-1-carrying vesicles co-transport CTNS-1

232   (21%), but this is lower than that observed in *lrk-1* mutants alone (45%) (Fig. 2B, 3D).

233

234   These data suggest that the axonal localization of SV-lysosomal compartments is dependent

235   on UNC-104 in wildtype and *apb-3* mutants but independent of UNC-104 in *lrk-1* mutants.

236   The extent of localization along the neuronal process in *apb-3* mutants is likely to reflect the

237   net transport activity of UNC-104. The SV-lysosomes in *lrk-1* likely depend on other motors

238   for their transport into axons, and in the absence of UNC-104, these alternate motors may

239   allow more SV-lysosomes to localize along the neuronal process. Additionally, UNC-104

240   may play an indirect role in the sorting of CTNS-1 from SNG-1 compartments in *lrk-1*

241   mutants.

242

243   **SV-lysosomes in *lrk-1* and *apb-3* mutants are differentially dependent on SYD-2**

244   The active zone protein SYD-2 has been shown to regulate lysosomal protein distribution in

245   *C. elegans* neurons (Edwards *et al.*, 2015a). SYD-2 is also a known genetic enhancer of

246   UNC-104 and is known to directly bind this motor (Zheng *et al.*, 2014; Shin *et al.*, 2003;

247   Wagner *et al.*, 2009; Stucchi *et al.*, 2018). We, therefore, examined whether the altered

248   localization of the SV-lysosomal compartments in *lrk-1* and *apb-3* depends on SYD-2. We

249   used two different alleles of *syd-2*, the null allele, *syd-2(ok217)*, and the loss-of-function

250   allele, *syd-2(ju37)*, with a premature stop codon in the LH2 domain (Zhen and Jin, 1999;

251   Wagner *et al.*, 2009). The N-terminal portion of SYD-2 expressed in *syd-2(ju37)* allele is

252   capable of physically associating with UNC-104 (Wagner *et al.*, 2009).

253

254   Both *syd-2(ok217)* and *syd-2*(*ju37*) resemble wildtype in the number of SNG-1-carriers co-

255   transporting CTNS-1 as well as in the number of animals showing CTNS-1 localization along

256   the PLM neuronal process (Fig. 4A and S1H, Movie S7). The co-transport of CTNS-1 in

257   SNG-1-carrying carriers is similar (~55–60%) in *lrk-1*, *apb-3*, and *lrk-1; syd-2(ok217)* mutant

258   animals (Fig. 4A; Suppl. Table 14). Similarly, the number of SNG-1-carriers co-transporting

259   RAB-7 in TRNs is comparable (~90%) in *lrk-1* and *lrk-1; syd-2(ok217)* mutant animals (Fig.

260   4B; Suppl. Table 15). Additionally, both *lrk-1; syd-2*(*ok217*) and *lrk-1; syd-2*(*ju37*) show an

261   increased or similar number of animals in which CTNS-1 or RAB-7 are localized along the

262   neuronal process compared to *lrk-1* alone (Fig. 4C, 4D, 4E and S1H). The number of animals

263   showing LMP-1 in the neuronal process in *lrk-1* and *lrk-1; syd-2*(*ok217*) is similar (Fig. 4F,

264   S1J, and S1K). Thus, SYD-2 does not appear to be required for the transport or localization

265   of SV-lysosomes. In the absence of SYD-2, more *lrk-1* animals show a greater number of

266   SV-lysosomes along the neuronal process, akin to the phenotypes observed in *lrk-1; unc-104*,

267   suggesting that SYD-2 might function like UNC-104.

268

269   In contrast to the above phenotypes observed with *lrk-1*, the number of SNG-1 carriers co-

270   transporting CTNS-1 or RAB-7 in *apb-3; syd-2(ok217)* (~40%) is similar to that in wildtype,

271   and is lower than that seen in *apb-3* mutants alone (Fig. 4A and 4B; Suppl. Tables 11 and

272   12). The number of animals with CTNS-1 and RAB-7 localized along the neuronal process is

273   lower in *apb-3; syd-2(ok217)* than in *apb-3* mutants (Fig. 4C, 4D, and S1H). Unlike these

274   markers, the number of LMP-1-marked carriers in the neuronal process of *apb-3; syd-*

275   *2(ok217)* is increased compared to that in *apb-3* mutants (Fig. 4F, S1J, and S1K). Further,

276   unlike in *apb-3; syd-2(ok217)*, the *apb-3; syd-2*(*ju37*) animals show increased co-transport of

277   CTNS-1 with SNG-1 (30%) compared to wildtype (10%) but lower than that in *apb-3*

278   mutants (63%) (Fig. 4A, Suppl. Tables 14 and 15). Furthermore, *lrk-1; syd-2*(*ju37*) and *apb-*

279   *3; syd-2(ju37)* show an increased number of animals with CTNS-1 localized along the

280   neuronal process compared to *lrk-1* and *apb-3* mutants, respectively (Fig. 4E and S1H). As

281   with *lrk-1* and *apb-3* mutants, the co-transport of CTNS-1 with either SNB-1 or RAB-3 is

282   unaffected in *syd-2(ok217)* (Fig. S3C and S3D; Suppl. Tables 16 and 17). As the *apb-3*

283   phenotypes appear to be dependent on the presence of SYD-2, it is likely that *syd-2* acts

284   downstream of *apb-3*. The genetic interaction of *apb-3* with the two *syd-2* alleles suggests

285   that the N-terminal region of SYD-2, which is known to bind UNC-104/KIF1A, is sufficient

286   to enable the exit of SV-lysosomes in the neuronal processes of *apb-3* mutants.

287

288   We next examined whether *syd-2* affects the composition of the SVp carrier pools without

289   lysosomal proteins. The incidence of co-transport of SNB-1 and RAB-3 is lower in *syd-*

290   *2(ok217)* mutants (~15%) than in wildtype (~35%) (Fig. 4G; Suppl. Table 18), similar to that

291   reported in *lrk-1* and *apb-3* single mutants (Choudhary *et al.*, 2017). Furthermore, *syd-*

292   *2(ok217)*, like *apb-3*, does not affect the co-transport of SNG-1 and RAB-3 (Fig. 4H; Suppl.

293   Table 19). These observations suggest that SYD-2 only affects the trafficking of a subset of

294   SVps and may act downstream of APB-3.

295

296   In *syd-2(ok217)*, the number of APB-3::GFP puncta per cell body increase (Fig. 2G, 2H and

297   S2G), while the size and average intensity of these puncta remain comparable to wildtype

298   animals (Fig. 2G(iii), 2I and 2J; Suppl. Tables 11 and 12). This suggests that *syd-2* may not

299   influence the ability of the AP-3 complex to associate with membrane surfaces, but rather

300   acts on the compartments formed after AP-3 has acted on them.

301

302   To further determine the hierarchy of action of SYD-2 on compartments formed in *lrk-1* and

303   *apb-3*, we examined *lrk-1 apb-3; syd-2* triple mutants. Notably, *lrk-1 apb-3; syd-2* triple

304   mutants are similar to *lrk-1 apb-3* in the co-transport of CTNS-1 with SNG-1 (Fig. 4A,

305   Suppl. Table 14). Furthermore, both *lrk-1 apb-3* double mutants and *lrk-1 apb-3*; *syd-2* triple

306   mutants show a similar number of animals with CTNS-1 compartments localized along the

307   neuronal process (Fig. 4A, 4C, and S1H). These data are consistent with a hierarchical

308   pathway wherein LRK-1 acts upstream of the AP-3 complex, and SYD-2 acts downstream of

309   AP-3 to facilitate UNC-104 activity.

310

311   **UNC-104 and SYD-2 are necessary for SV-lysosome transport in *apb-3* mutants**

312   Previous studies have shown that the N-terminal region of Liprin-α/SYD-2 binds to

313   KIF1A/UNC-104 (Shin *et al*., 2003; Wagner *et al*., 2009; Stucchi *et al*., 2018). This physical

314   interaction between SYD-2 and UNC-104, in addition to the genetic interactions that we and

315   others observe, suggests that SYD-2 may act through UNC-104 to facilitate both motor and

316   its cargo's transport (Wagner *et al*., 2009; Zheng *et al*., 2014). Further, we have shown that

317   SVp carriers in mutants of *lrk-1* and *apb-3* are only partially dependent on UNC-104 for their

318   transport (Choudhary *et al*., 2017). Therefore, we examined the potential role of the UNC-

319   104–SYD-2 complex in the localization and transport of SVp carriers and SV-lysosomes.

320

321   In wildtype animals, the localization of the transmembrane SVp SNG-1 is dependent on

322   UNC-104 but not on SYD-2 (Fig. 3B and 5B). However, *unc-104*; *syd-2* mutants have less

323   SNG-1 in the PLM neuronal process compared to that seen in *unc-104* single mutants,

324   demonstrating that SYD-2 facilitates UNC-104-dependent SVp transport (Fig. 5B) (Zheng *et*

325   *al*., 2014). Transport of SVps is not dependent on SYD-2 in either *lrk-1* or *apb-3* mutants

326   (Fig. 5B). *lrk-1*; *unc-104* and *lrk-1*; *unc-104*; *syd-2* triple mutants show comparable SNG-1

327   localization in the neuronal process. Likewise, *apb-3*; *unc-104* and *apb-3*; *unc-104*; *syd-2*

328   also show comparable SNG-1 localization along the neuronal process (Fig. 5B). However, in

329   *lrk-1*; *unc-104*; *syd-2* triple mutants, the peripherally-associated membrane protein RAB-3

330   does not reach the synapse unlike in *lrk-1*; *unc-104* double mutants (Fig. S3A). Unlike the

331   phenotypes with *lrk-1*, RAB-3 localization in *apb-3*; *unc-104*; *syd-2* and *apb-3*; *unc-104* is

332   similar (Fig. S3A). Together, these data indicate that SYD-2 does not facilitate UNC-104-

333   dependent SVp transport in *apb-3* mutants.

334

335   SV-lysosomes, marked by CTNS-1, are dependent on UNC-104 and largely independent of

336   SYD-2 in wildtype (Fig. S3B). The number of SNG-1 vesicles co-transporting CTNS-1 is

337   similar in *unc-104*, *syd-2*, and *unc-104*; *syd-2* mutant animals (Fig. 5D; Suppl. Table 20),

338   suggesting that these genes do not regulate the sorting of lysosomal and SV proteins away

339   from each other.

340

341   In *lrk-1* mutants, SV-lysosomes are independent of SYD-2 and UNC-104 (Fig. 3C). *lrk-1*;

342   *unc-104* and *lrk-1*; *unc-104*; *syd-2* triple mutants show comparable localization of CTNS-1

343   along the neuronal process (Fig. S1H), suggesting that SYD-2 does not facilitate UNC-104-

344   dependent SV-lysosome trafficking in *lrk-1* mutants. The CTNS-1-marked SV-lysosomes in

345   *apb-3* mutants are dependent on both UNC-104 and SYD-2 (Fig. 3C and 5C). The *apb-3*;

346   *unc-104*; *syd-2* triple mutants are similar to the *apb-3; unc-104* and *apb-3; syd-2* mutants

347   (Fig. 5C and S1H). These data suggest that SYD-2 is important for the localization of the SV-

348   lysosomal compartments along the neuronal process in *apb-3* mutants.

349

350   SVp carriers depend on both UNC-104 and SYD-2 in wildtype, but the SNG-1-containing

351   compartment only partially depends on UNC-104 but not SYD-2 in both *lrk-1* and *apb-3*

352   mutants. SV-lysosomes depend on UNC-104 but appear to be largely independent of SYD-2

353   in wildtype. In *lrk-1* mutants, the SV-lysosomes appear to be independent of both UNC-104

354   and SYD-2. In *apb-3* mutants, SV-lysosomes are dependent on both UNC-104 and SYD-2.

355   This suggests that, in *apb-3* mutants, the preference for the UNC-104-SYD-2 complex is

356   switched between the SVp alone-containing compartments (both SNG-1 and RAB-3) and the

357   SV-lysosomes. The action of AP-3 appears essential to ensure that SYD-2 facilitates UNC-

358   104-dependent transport of SVps.

359

360   **SYD-2 and the AP-1 complex together regulate the polarized distribution of SVps**

361   SNB-1-labeled SVp carriers in *lrk-1* and *apb-3* have been shown to mislocalize to the

362   dendrites (Sakaguchi-Nakashima *et al.*, 2007; Choudhary *et al.*, 2017). Since *syd-2*

363   phenocopies *lrk-1* and *apb-3* in affecting the co-transport of SNB-1 and RAB-3 (Fig. 4G)

364   (Choudhary *et al.*, 2017), we examined whether SVps mislocalize to dendrites in *syd-2*

365   mutants. Similar to wildtype, SNB-1 was found to be excluded from the dendrites of the ASI

366   neuron in *syd-2(ok217)* (Fig. 6B, Table 1), which shows a similar orientation of axonal and

367   dendritic microtubules as wildtype (Fig. S4A). Thus, SYD-2 does not appear to play a key

368   role by itself in regulating polarized trafficking of SVps.

369

370   Previous studies have shown that the dendritic mislocalization of SNB-1 in *lrk-1* depends on

371   the UNC-101/μ subunit of the AP-1 complex (Sakaguchi-Nakashima *et al.*, 2007; Choudhary

372   *et al.*, 2017). Therefore, we examined whether *syd-2* genetically interacts with *unc-101* to

373   regulate the polarized distribution of SVps. SNB-1 is absent from dendrites in *syd-2* and *unc-*

374   *101* single mutant animals, while *unc-101*; *syd-2(ok217)* fails to exclude SNB-1 from the ASI

375   dendrite (Fig. 6B). Further, SNB-1 dendritic mislocalization is suppressed in *lrk-1*; *syd-*

376   *2(ok217)* and *apb-3*; *syd-2(ok217)* mutants (Fig. 6B; Table 1), suggesting that the dendritic

377   mislocalization of SNB-1 in *lrk-1* and *apb-3* depends on SYD-2. Unlike the null allele *syd-*

378   *2(ok217)*, the loss-of-function allele *syd-2(ju37)* does not suppress the dendritic

379   mislocalization of SNB-1 to the ASI dendrite in *lrk-1* and *apb-3* mutants (Fig. 6B). SYD-2

380   appears to act redundantly with the AP-1 complex to regulate polarized SVp trafficking.

381   Additionally, SYD-2 acts similarly to the AP-1 complex to facilitate SVp entry into dendrites

382   in *lrk-1* and *apb-3* mutants.

383

384   We also assessed CTNS-1 localization in dendrites and found that only *lrk-1* shows a

385   significant increase in the number of dendritic CTNS-1 puncta, while *apb-3*, *syd-2(ok217)*,

386   *unc-101*, and *unc-101; syd-2* are all similar to wildtype (Fig. 6C and 6D). We then assessed

387   whether SYD-2 regulates the trafficking of dendritic cargo, which are known to depend on

388   UNC-101 (Dwyer *et al.*, 2001). Both *unc-101* and *apb-3* show mislocalization of the ODR-

389   10::GFP receptor to the AWC axon, while wildtype and *syd-2* mutants localize ODR-

390   10::GFP only along the AWC dendrite and at the dendritic tip (Fig. S4B). We previously

391   showed that UNC-101 regulates the length of the SVp carriers that exit the neuronal cell

392   bodies (Choudhary *et al.*, 2017). *unc-101* mutants form longer SVp carriers than that seen in

393   wildtype; however, *syd-2* does not alter the longer SVp carrier length seen in *unc-101*

394   mutants (Fig. S4C).

395

396   These data suggest that *syd-2* and *unc-101* are genetically redundant in preventing SVp entry

397   into dendrites but *syd-2* does not alter the axonal phenotypes of *unc-101*. Additionally, the

398   SYD-2 LH1 domain is likely sufficient to enable dendritic entry of atypical SVp carriers

399   formed in *lrk-1* and *apb-3* mutants. Furthermore, *lrk-1* seems to have wider dendritic

400   trafficking defects than those seen in *apb-3*.

401

402   **SYD-2 alters the localization of UNC-101 in head neurons**

403   As previously reported, the localization of UNC-101 on the Golgi is altered in *lrk-1* mutants

404   (Choudhary *et al.*, 2017) (Fig. 6F). Thus, we examined if *syd-2* alters the localization of

405   UNC-101::GFP in the cell bodies of neurons in the head ganglia (Fig. 6E). The UNC-

406   101::GFP puncta are fainter and smaller (Fig. 6F, 6G and 6H; Suppl. Tables 21 and 22), and a

407   higher percentage of cell bodies have no or fewer puncta in the head neurons in *syd-2*

408   mutants as compared to that in wildtype (Fig. S4D, Suppl. Table 23). In ventral cord neurons,

409   *syd-2* affects the intensity of UNC-101::GFP puncta (Fig. 6I and 6J; Suppl. Table 24). Thus,

410   SYD-2 alters the localization of UNC-101 in *C. elegans* neurons, which might account for its

411   role in suppressing the dendritic mistrafficking of some SVps in head neurons.

412

413   Further, the loss-of-function allele of *syd-2*, *syd-2(ju37)*, did not alter the intensity or size of

414   UNC-101::GFP puncta (Fig. S4E, F, and G; Suppl. Tables 25 and 26). This suggests that the

415   SYD-2 N-terminus domain is sufficient for AP-1 localization.

Discussion

Our study, like others, shows that SVps are trafficked in many heterogenous carriers and sometimes with lysosomal proteins, suggesting that SVps and lysosomal proteins share trafficking routes (Figs. 1A,1B, 2B, and 2C) (Maeder, Shen and Hoogenraad, 2014; Newell-Litwa *et al*., 2009; Vukoja *et al*., 2018). LRK-1 and, as reported earlier, the AP-3 complex, help in sorting SVps away from lysosomal proteins (Figs. 2B and 2C) (Newell-Litwa *et al*., 2009). In addition, *lrk-1* mutant animals appear to have more widespread trafficking defects of both SVps and lysosomal proteins in comparison to *apb-3* mutants (Fig. 2A and 2F). UNC-104 requires SYD-2 to facilitate the transport of SV carriers that lack lysosomal proteins in wildtype (Fig. 5B) (Zheng *et al*., 2014). The SV-lysosome carrier is dependent on UNC-104, but is largely independent of SYD-2 in wildtype (Fig. S3B). However, in the absence of the AP-3 complex, the preference is switched such that the SV-lysosomes depend on both UNC-104 and SYD-2, but the SVs are only partially dependent on UNC-104 and independent of SYD-2 (Fig. 3B, 3C, 5B, 5C and S3A). Some effects on SYD-2 are likely to be mediated via AP-3 localization to membrane surfaces, perhaps working in concert with UNC-104 to regulate the kinetics of AP-3 membrane cycling. The polarized trafficking of SVps appears to require either SYD-2 or UNC-101, which act redundantly with each other likely due to the role of SYD-2 in enabling localization of the AP-1 complex to the Golgi (Fig. 6B).

LRRK2 is known to affect the trafficking of lysosomal proteins (Kuwahara *et al*., 2016; Piccoli and Volta, 2021; Inoshita *et al*., 2022), SVps (Sakaguchi-Nakashima *et al*., 2007; Cirnaru *et al*., 2014; Choudhary *et al*., 2017), retromer and ER-Golgi proteins (Xiong *et al*., 2012; MacLeod *et al*., 2013; Linhart *et al*., 2014), dense core vesicle proteins (Inoshita *et al*., 2022), RAB GTPases (Steger *et al*., 2016; Lanning *et al*., 2018; Madero-Pérez *et al*., 2018),

441   neurotransmitter transporters (Iovino *et al*., 2022), autophagy-related proteins LC3 and

442   LAMP-1 (Wallings, Connor-Robson and Wade-Martins, 2019), and mitochondria (Weindel

443   *et al*., 2020). The trafficking and localization of lysosomal proteins via LRRK2 seem to

444   depend on RAB-7 and the retromer complex (Dodson *et al*., 2012; Vilariño-Güell *et al*.,

445   2011; Zimprich *et al*., 2011). AP-3 is also known to play a key role in sorting lysosomal

446   proteins in a variety of cells and separating SVps from lysosomal proteins at a common

447   trafficking compartment (Salazar *et al*., 2004; Newell-Litwa *et al*., 2009; Kuwahara *et al*.,

448   2016). Additionally, the *C. elegans* AP-3 complex is shown to be a downstream effector of

449   LRK-1/LRRK2 in axon outgrowth and the co-transport of SNB-1 and RAB-3 along the

450   neuronal process (Kuwahara *et al*., 2016; Choudhary *et al*., 2017). *lrk-1* mutants show more

451   widespread trafficking defects than *apb-3* mutants, such as the presence of LMP-1 along the

452   neuronal process, the presence of CTNS-1 in the dendrite, and reduced cotransport of SNG-1

453   with RAB-3 (Fig. 2A, 2F and 6C). *lrk-1* and *apb-3* mutants appear to share all other

454   remaining phenotypes, notably that many more SNG-1-transport carriers contain CTNS-1,

455   while nearly all CTNS-1 carriers continue to carry SNG-1 as seen in wildtype (Fig. S2B).

456   The AP-2 complex is reported to regulate the trafficking of LAMP-1 and LAMP-2 to the

457   lysosomes via the plasma membrane, while the AP-3 complex has little effect on their

458   trafficking (Janvier and Bonifacino, 2005); this supports our data that trafficking of LMP-1 is

459   likely mediated by LRRK2 independently of the AP-3 complex. Thus, LRK-1 may act

460   upstream of AP-3; however, our data do not fully exclude the possibility that LRK-1 and AP-

461   3 act additively to regulate the localization of a subset of lysosomal markers (Fig. S1H-K).

462

463   The AP-3 complex can physically bind to LRRK2 (Kuwahara *et al*., 2016; Heaton *et al*.,

464   2020). Therefore, some of the trafficking defects seen in *lrk-1* may occur through its ability to

465   affect the efficient recruitment of the AP-3 complex to membrane surfaces (Fig. 2G-J), as has

466   already been seen for AP-1 (Choudhary *et al*., 2017). Phosphorylation of the AP-3 complex

467   has been shown to be necessary to recruit on SVs and to play a role in endosomal SV

468   biogenesis (Faundez and Kelly, 2000). Further, LRRK2 has been shown to physically interact

469   with the AP-2 complex via its ROC domain (Heaton *et al*., 2020). The LRRK2 ROC domain

470   regulates the LRRK2 kinase activity (Deng *et al*., 2008). Therefore, LRRK2, via its kinase

471   activity (Heaton *et al*., 2020), could regulate AP-3's localization or activity. Alternatively,

472   LRK-1 could alter the composition of membrane compartments (Piccoli and Volta, 2021) and

473   indirectly affect the recruitment and function of the AP-3 complex.

474

475   UNC-104/KIF1A is a critical motor for transporting SVps (Hall and Hedgecock, 1991;

476   Okada and Hirokawa, 1999; Pack-Chung *et al*., 2007). The SV-lysosomes in wildtype,

477   although dependent on UNC-104, do not extend very far into the axon (Fig. 3C, S1H and

478   S3B), perhaps because they have fewer numbers of UNC-104 motors on their surface

479   compared to SVp carriers lacking lysosomal proteins. In *lrk-1* and *apb-3* mutants, SVs

480   partially depend on UNC-104 (Fig. 3B and S3A) (Choudhary *et al*., 2017). It is likely that in

481   *lrk-1* mutants, both SVs and SV-lysosomes depend on multiple motors for their axonal

482   transport, much like that seen in *unc-16* mutants, where UNC-16 acts upstream of LRK-1

483   (Byrd *et al*., 2001; Brown *et al*., 2009; Choudhary *et al*., 2017). However, *syd-2* mutants,

484   despite sharing some SVp trafficking defects with *lrk-1* and *apb-3* mutants (Fig. 4G and 4H),

485   retain UNC-104 dependence for both SV and SV-lysosome transport (Fig. S3A, 5B and 5C).

486

487   SYD-2 is thought to physically associate with the motor, cluster UNC-104, and regulate

488   motor processivity (Shin *et al*., 2003; Wagner *et al*., 2009; Zheng *et al*., 2014; Stucchi *et al*.,

489   2018). The clustering of UNC-104 and increase in processivity might account for the UNC-

490   104 dependence of SVp transport on SYD-2. The effect of SYD-2 on UNC-104-dependent

491 transport may rely on the pre-existing numbers of UNC-104 on the cargo surface. A larger

492 number of motors on the cargo surface may be more sensitive to the UNC-104-clustering

493 activity of SYD-2. Active zone proteins like Piccolo and Bassoon have been thought to

494 cluster vesicles, although some studies suggest that such active zone proteins can be

495 transported in carriers along with SVps (Jin and Garner, 2008; Goldstein, Wang and

496 Schwarz, 2008; Maas *et al*., 2012). SYD-2 is both an UNC-104 interactor and an active zone

497 protein (Zhen and Jin, 1999; Zheng *et al*., 2014). *syd-2* mutants do not show major changes in

498 the localization of SVps or lysosomal proteins and the degree of co-transport of most SV and

499 lysosomal markers assessed (Fig. 4A-D, 4F-H, 5B and S3C-D). This suggests that SYD-2,

500 despite interacting with UNC-104, does not have major roles in the transport or localization

501 of membrane cargo by itself. However, its role is uncovered when there is a reduction in the

502 levels of UNC-104 motor, particularly in the transport of SVs (Fig. 5B and S3A). The

503 reduction in the transport of SV-lysosomes in *apb-3* depends on the presence of an UNC-

504 104-interacting domain of SYD-2 (Fig. 4A, note *apb-3*; *syd-2(ju37)*). In the absence of SYD-

505 2's UNC-104-interacting domain, UNC-104 may not effectively cluster on the surface of SV-

506 lysosomes and therefore, transport of these compartments is reduced. Thus, we think that our

507 data can be explained by SYD-2's action with UNC-104 rather than a clustering role for

508 multiple vesicles. A role of SYD-2 via regulating the balance/activity of microtubule-

509 dependent motors has also been proposed in lysosome localization in motor neurons of *C*.

510 *elegans* (Edwards *et al*., 2015b).

511

512 Localization of the AP complexes is altered in *syd-2* mutants (Fig. 2G-J, S2G, 6F-H, S4D).

513 There are more and brighter APB-3 puncta in *syd-2*, while there are fewer, less bright, and

514 smaller UNC-101 puncta in *syd-2* animals. The effects of SYD-2 on APB-3 may be explained

515 in two ways. AP-3 recruitment to membrane surfaces depends on binding to cargo proteins

516   (Schoppe *et al*., 2021). Therefore, after AP-3 has sorted cargo, SYD-2 may facilitate UNC-

517   104 clustering, and thereby permit sufficient force generation to enable exit of cargo proteins

518   from an endosomal compartment. Multiple motors are known to generate greater pulling

519   force and deformation of membrane compartments (Roux *et al*., 2002; Du *et al*., 2016).

520   Moreover, the Kinesin 3 family motor KIF13A has been shown to physically bind the AP-1

521   complex to regulate trafficking of mannose-6-phosphate receptor and the melanosomal cargo,

522   Tyrp1, through affecting AP-1 localization (Nakagawa *et al*., 2000; Delevoye *et al*., 2014).

523   SYD-2's action may facilitate a similar role of UNC-104 in trafficking. An alternate

524   possibility is that the kinetics of sorting is affected in the absence of SYD-2, leading to

525   persistence of AP-3 complexes on membrane surfaces observed as an increase in the number

526   of puncta in *syd-2* mutants. It is unclear how SYD-2 might influence the recruitment of the

527   AP-1 complex to the membrane. One possibility is that the changes in the AP-3 localization

528   and potential changes in flux through the secretory pathway lead to slowing down of

529   trafficking and therefore changes in localization of AP-1 to reduce cargo jamming in Golgi

530   and post-Golgi compartments.

531

532   Polarized trafficking of SVps, specifically their exclusion from dendrites, is dependent on

533   both LRK-1 and the AP-3 complex. SNB-1 mistrafficking in both *lrk-1* and *apb-3* mutants is

534   dependent on SYD-2 as well as the AP-1 complex (Fig. 6B) (Sakaguchi-Nakashima *et al*.,

535   2007; Choudhary *et al*., 2017). The role of SYD-2 in preventing SNB-1 from entering the

536   dendrite in *lrk-1* and *apb-3* mutants might be due to the reduced levels of AP-1 on the Golgi

537   (Fig. 6G, 6H, and 6J). Therefore, in the allele of *syd-2* that does not affect AP-1 localization,

538   *syd-2(ju37)*, *lrk-1* and *apb-3* mutants continue to mistraffick SNB-1 to dendrites (Fig. S4E, F

539   and G). The mistrafficking of SNB-1 into dendrites of *unc-101*; *syd-2* double mutants may be

540 akin to the dendritic mislocalization of SVp in *unc-104* mutants (Yan *et al*., 2013). The lack

541 of sufficient UNC-104 activity may permit dynein motors to enable dendritic entry of SVps.

542

543 In conclusion, we propose that in the SV biogenesis pathway, one key step is the separation

544 of SVps from lysosomal proteins via LRK-1 and the AP-3 complex. We also propose a novel

545 role for the active zone protein SYD-2 as a regulator of SVp trafficking, acting downstream

546 to the AP-3 complex and via UNC-104, and as a regulator of polarized distribution of SVps

547 acting along with the AP-1 complex. We show that SYD-2 genetically interacts with and

548 alters the localization of both the AP-3 and AP-1 complexes to regulate the transport and

549 polarized distribution of SVp carriers in *C. elegans* neurons.

550

560

561

562 **Materials and methods**

563 **Strain maintenance**

564 *C. elegans* strains were grown and maintained at 20 °C on NGM plates seeded with *E. coli*

565 OP50 strain using standard methods (Brenner, 1974). BD Bacto-Petone and BD Agar for the

566 NGM were sourced from Becton, Dickinson and Company NJ, USA. All Sigma salts and

567 Sigma cholesterol were obtained from local distributors of Sigma and Merck products. L4 or

568 1-day adult animals were used for imaging in all cases. The strains used are listed in

569 Supplementary Table 1. Some strains were provided by the CGC, which is funded by NIH

570 Office of Research Infrastructure Programs (P40 OD010440).

571

572 **Plasmid construction**

573 Expression plasmids were generated using standard PCR-based subcloning techniques. The

574 *mec-4*p::*ctns-1*::*mCherry* plasmid (TTpl 509) was generated by replacing the *unc-129*p from

575 #KG371 (Edwards *et al.*, 2013) with *mec-4*p using *Hind*III and *Bam*HI restriction enzymes.

576 The *str-3*p::*ctns-1*::*mCherry* was generated by replacing the *unc-129*p from #KG371 with *str-*

577 *3*p using *Bam*HI and *Apa*I restriction sites. To generate the *mec-4*p::*sng-1*::*gfp* plasmid (TTpl

578 696), SNG-1::GFP was amplified from NM491 (Zhao and Nonet, 2001) and cloned into a

579 *mec-4*p containing vector using *Nhe*I and *Eco*RV restriction sites. To generate *rab-3*p::*apb-*

580 *3*::*gfp* (TTpl 796), APB-3 was amplified from genomic DNA using Phusion Polymerase and

581 cloned into a *rab-3*p-containing vector using *Nhe*I and *Age*I restriction sites. To generate

582 touch neuron specific expression plasmids for *rab-7* and *lmp-1* under the *mec-7* promoter

583 (Hamelin *et al.*, 1992), cloning was performed using the Gateway *in vitro* recombination

584 system (Invitrogen, Carlsbad, CA) using Grant lab modified versions of MiniMos enabled

585 vectors pCFJ1662 (Hygromycin resistant) and pCFJ910 (G418 resistant) (gifts of Erik

586 Jorgensen, University of Utah, Addgene #51482): pCFJ1662 Pmec7 GTWY mNeonGreen

587   let858 (34F6) or pCFJ1662 Pmec7 mNeonGreen GTWY let858 (34D4), and pCFJ910 Pmec7

588   mScarleti GTWY let858 (33B6). pDONR221 entry vectors containing coding regions for

589   *lmp-1* and *rab-7* were recombined into neuronal destination vectors by Gateway LR clonase

590   II reaction to generate C-/N- terminal fusions. Single-copy integrations were obtained by

591   MiniMOS technology (Frøkjaer-Jensen *et al*., 2008).

592

593   **Generation of transgenic *C*. *elegans***

594   Transgenic lines were generated by following standard microinjection procedure (Fire *et al*.,

595   1998) using an Olympus Ix53 microscope equipped with 20× and 40× lenses, Narishige M-

596   152 micromanipulator (Narishige, Japan), and Eppendorf Femtojet 2 microinjector (local

597   distributors of Eppendorf products). The F2 progeny that inherited and stably expressed the

598   extrachromosomal transgene were UV irradiated to generate integrated lines. Worms

599   showing 100% transmission were selected and outcrossed with the wildtype N2 strain five

600   times. Detailed information on the concentration of plasmids and co-injection markers used is

601   listed in Supplementary Table 2.

602

603   **Imaging**

604   **(i)**   **Static imaging:** L4 or 1-day adult worms were immobilized using 30 mM sodium

605   azide and mounted on 2–5% agarose pads. Images were acquired on an Olympus

606   IX73 Epifluorescence microscope with an Andor EMCCD camera or the Olympus

607   Fluoview FV1000 confocal laser scanning microscope or Olympus IX83 with

608   Perkin Elmer Ultraview Spinning Disc confocal microscope fitted with a

609   Hamamatsu EMCCD camera. Since AP-3 localization is sensitive to levels of

610   ATP (Faundez and Kelly, 2000), static imaging of APB-3::GFP was performed

611   using 5 mM Tetramisole. APB-3::GFP was imaged on Olympus Spin SR10

612   (SoRA, 50 μm disk) fitted with Teledyne Photometrics sCMOS camera.

613   **(ii)**   **Time-lapse imaging:** L4 worms were anesthetized in 3 mM tetramisole (Sigma-

614   Aldrich) and mounted on 5% agarose pads. Time-lapse images were acquired in

615   Olympus IX83 with Perkin Elmer Ultraview Spinning Disc confocal microscope

616   and a Hamamatsu EMCCD camera or the Olympus Fluoview FV1000 confocal

617   laser scanning microscope. Dual color simultaneous imaging was performed at 3

618   frames per second (fps), dual color sequential imaging was done at 1.3 fps, and

619   single fluorophore imaging for analysis of vesicle length was done at 5 fps. All

620   movies were 3 minutes long, and the region of imaging in the PLM comprised the

621   first 60–100 μm of the neuronal process immediately outside the cell body, with

622   the cell body in the frame of imaging. Live imaging of EBP-2::GFP to assess

623   microtubule polarity was carried out using an Olympus IX73 Epifluorescence

624   microscope with an Andor EMCCD camera at 3 fps.

625

626   **Analysis**

627   All analysis was done using FIJI (Schindelin *et al*., 2012).

628   **(i) Co-migration analysis:** Kymographs were generated from identical regions of the movie

629   in both color channels utilizing the ImageJ plugin MultipleKymograph. The kymographs

630   were then synchronized and the overlapping sloped lines were considered as co-migrating

631   particles. For dual-color co-migration analysis, number of moving vesicles were counted

632   which were positive for GFP alone, RFP alone, and vesicles positive for both GFP and RFP.

633   Total number of vesicles = number of vesicles positive only for GFP + number of vesicles

634   only positive for RFP + number of vesicles positive for both GFP and RFP.

635    $\% \text{ co-migrating vesicles} = [\frac{\text{Number of vesicles positive for both GFP and RFP}}{\text{Total number of vesicles}}] \text{ x } 100$

636   Fraction of GFP-positive vesicles co-migrating with RFP-positive vesicles =

637    $[\frac{\text{Number of vesicles positive for both GFP and RFP}}{\text{Number of vesicles only positive for GFP+Number of vesicles positive for both GFP and RFP}}]$

638   For detailed methods, please refer to (Nadiminti and Koushika, 2022).

639   **(iii) Quantitation of penetrance of CTNS-1 puncta that exit into PLM neurites:** For each

640   genotype, at least 30 animals were annotated to observe the extent of CTNS-1 (or RAB-7 or

641   LMP-1) presence in the PLM major neurite. Penetrance was measured by calculating the

642   number of animals in which CTNS-1 (or RAB-7 or LMP-1) was present at or beyond the first

643   25 μm and 50 μm away from the cell body.

644   **(iv) Quantitating the direction of motion of CTNS-1-carrying compartments:** Only

645   moving CTNS-1-carrying compartments were analyzed for their direction of motion. For

646   CTNS-1-marked compartments moving clearly in a particular direction, they were annotated

647   as such. For those moving bidirectionally, their net displacement was used to identify their

648   direction of motion. If the vesicle's final position at the end of the kymograph was closer to

649   the cell body than when it started, it was considered to have moved retrogradely. If the

650   vesicle's final position at the end of the kymograph was farther away from the cell body than

651   when it started, it was considered to have moved anterogradely. For vesicles whose position

652   at the end of the kymograph remained largely unchanged, they were either not considered for

653   analysis or were assigned the direction in which they were moving immediately before the

654   end of the kymograph, depending upon how discernible their direction of motion was.

655

656   **(iv) Density of CTNS-1 in the ASI dendrite:** The number of CTNS-1 puncta in the dendrite

657   and the length of measurable region (ROI) in the dendrite from the cell body to the end was

658   counted for each animal. The density of lysosomes per 10 μm was calculated as:

659   [Number of CTNS-1 puncta in the dendrite/Length of the dendrite ROI] × 10

660   **(iv) Quantitation of intensity of UNC-101::GFP and APB-3::GFP puncta:** For UNC-

661   101::GFP, two regions were chosen – (i) the cell bodies of the head neuron ganglia and (ii)

662   the cell bodies along the ventral nerve cord. For APB-3::GFP, neurons in three regions – the

663   head, along the ventral cord, and the tail – were analyzed. For both UNC-101::GFP and APB-

664   3::GFP, per cell body, the number of puncta was calculated on a plane with the best focus for

665   that cell body. On the same plane, the size and intensity of each puncta were measured. A

666   cytosolic region close to one of the puncta was chosen to measure puncta/cytosolic intensity.

667   Puncta intensity was quantitated by dividing the intensity of each puncta by the cytosolic

668   intensity. All the values of puncta intensity to cytosolic intensity per cell body were averaged

669   and plotted.

670

671   **(v) Vesicle length analysis:** In every kymograph, random non-overlapping ROIs (regions of

672   interest) were chosen to measure the size of the vesicles. These random ROIs were generated

673   by [Macro 1]. Any macro-generated random ROI that overlapped with a previous ROI for

674   that kymograph was not used for the analysis. Within each ROI, the length of each moving

675   compartment was quantified by measuring the thickness of the sloped line along the x-axis.

676   Such measurements were done at regions not overlapping with stationary particles or other

677   moving particles.

678   **(vi) Microtubule polarity:** Kymographs were generated from live movies of EBP-2::GFP in

679   the axonal and anterior dendritic regions of the PVD neuron imaged at 3 fps. The number of

680   anterogradely and retrogradely moving EBP-2 were counted from the kymographs and

681   plotted.

682   **Statistical analysis**

683   All statistical analyses were performed using OriginLab 2019. Distributions were checked

684   for normality using the Shapiro–Wilk test. Data that fit a normal distribution were compared

685   using one-way ANOVA with Tukey's post-hoc test. Data that did not fit a normal distribution

686   were compared using the Mann–Whitney test. Differences were considered significant when

687   the p-value < 0.05.

References:

Aravamudan, B., Fergestad, T., Davis, W. S., Rodesch, C. K. and Broadie, K. (1999) 'Drosophila UNC-13 is essential for synaptic transmission', *Nat Neurosci*, 2(11), pp. 965-71.

Brenner, S. (1974) 'The genetics of Caenorhabditis elegans', *Genetics*, 77(1), pp. 71-94.

Brockmann, M. M., Zarebidaki, F., Camacho, M., Grauel, M. K., Trimbuch, T., Südhof, T. C. and Rosenmund, C. (2020) 'A Trio of Active Zone Proteins Comprised of RIM-BPs, RIMs, and Munc13s Governs Neurotransmitter Release', *Cell Rep*, 32(5), pp. 107960.

Brown, H. M., Van Epps, H. A., Goncharov, A., Grant, B. D. and Jin, Y. (2009) 'The JIP3 scaffold protein UNC-16 regulates RAB-5 dependent membrane trafficking at C. elegans synapses', *Dev Neurobiol*, 69(2-3), pp. 174-90.

Bury, L. A. D. and Sabo, S. L. (2011) 'Coordinated trafficking of synaptic vesicle and active zone proteins prior to synapse formation', *Neural Development*, 6(1), pp. 24.

Byrd, D. T., Kawasaki, M., Walcoff, M., Hisamoto, N., Matsumoto, K. and Jin, Y. (2001) 'UNC-16, a JNK-signaling scaffold protein, regulates vesicle transport in C. elegans', *Neuron*, 32(5), pp. 787-800.

Choudhary, B., Kamak, M., Ratnakaran, N., Kumar, J., Awasthi, A., Li, C., Nguyen, K., Matsumoto, K., Hisamoto, N. and Koushika, S. P. (2017) 'UNC-16/JIP3 regulates early events in synaptic vesicle protein trafficking via LRK-1/LRRK2 and AP complexes', *PLOS Genetics*, 13(11), pp. e1007100.

Cirnaru, M. D., Marte, A., Belluzzi, E., Russo, I., Gabrielli, M., Longo, F., Arcuri, L., Murru, L., Bubacco, L., Matteoli, M., Fedele, E., Sala, C., Passafaro, M., Morari, M., Greggio, E., Onofri, F. and Piccoli, G. (2014) 'LRRK2 kinase activity regulates synaptic vesicle trafficking and neurotransmitter release through modulation of LRRK2 macro-molecular complex', *Frontiers in molecular neuroscience*, 7, pp. 49-49.

Dai, Y., Taru, H., Deken, S. L., Grill, B., Ackley, B., Nonet, M. L. and Jin, Y. (2006) 'SYD-2 Liprin-alpha organizes presynaptic active zone formation through ELKS', *Nat Neurosci*, 9(12), pp. 1479-87.

Delevoye, C., Miserey-Lenkei, S., Montagnac, G., Gilles-Marsens, F., Paul-Gilloteaux, P., Giordano, F., Waharte, F., Marks, M. S., Goud, B. and Raposo, G. (2014) 'Recycling endosome tubule morphogenesis from sorting endosomes requires the kinesin motor KIF13A', *Cell reports*, 6(3), pp. 445-454.

Deng, J., Lewis, P. A., Greggio, E., Sluch, E., Beilina, A. and Cookson, M. R. (2008) 'Structure of the ROC domain from the Parkinson's disease-associated leucine-rich repeat kinase 2 reveals a dimeric GTPase', *Proceedings of the National Academy of Sciences*, 105(5), pp. 1499-1504.

Dodson, M. W., Zhang, T., Jiang, C., Chen, S. and Guo, M. (2012) 'Roles of the Drosophila LRRK2 homolog in Rab7-dependent lysosomal positioning', *Human molecular genetics*, 21(6), pp. 1350-1363.

Du, W., Su, Q. P., Chen, Y., Zhu, Y., Jiang, D., Rong, Y., Zhang, S., Zhang, Y., Ren, H., Zhang, C., Wang, X., Gao, N., Wang, Y., Sun, L., Sun, Y. and Yu, L. (2016) 'Kinesin 1 Drives Autolysosome Tubulation', *Dev Cell*, 37(4), pp. 326-336.

Dwyer, N. D., Adler, C. E., Crump, J. G., L'Etoile, N. D. and Bargmann, C. I. (2001) 'Polarized Dendritic Transport and the AP-1 µ1 Clathrin Adaptor UNC-101 Localize Odorant Receptors to Olfactory Cilia', *Neuron*, 31(2), pp. 277-287.

Edwards, S. L., Morrison, L. M., Yorks, R. M., Hoover, C. M., Boominathan, S. and Miller, K. G. (2015a) 'UNC-16 (JIP3) Acts Through Synapse-Assembly Proteins to Inhibit the Active Transport of Cell Soma Organelles to Caenorhabditis elegans Motor Neuron Axons', *Genetics*, 201(1), pp. 117-141.

Edwards, S. L., Morrison, L. M., Yorks, R. M., Hoover, C. M., Boominathan, S. and Miller, K. G. (2015b) 'UNC-16 (JIP3) Acts Through Synapse-Assembly Proteins to Inhibit the Active Transport of Cell Soma Organelles to Caenorhabditis elegans Motor Neuron Axons', *Genetics*, 201(1), pp. 117-41.

Edwards, S. L., Yu, S. C., Hoover, C. M., Phillips, B. C., Richmond, J. E. and Miller, K. G. (2013) 'An organelle gatekeeper function for Caenorhabditis elegans UNC-16 (JIP3) at the axon initial segment', *Genetics*, 194(1), pp. 143-61.

Faundez, V. V. and Kelly, R. B. (2000) 'The AP-3 complex required for endosomal synaptic vesicle biogenesis is associated with a casein kinase Ialpha-like isoform', *Molecular biology of the cell*, 11(8), pp. 2591-2604.

Fire, A., Xu, S., Montgomery, M. K., Kostas, S. A., Driver, S. E. and Mello, C. C. (1998) 'Potent and specific genetic interference by double-stranded RNA in Caenorhabditis elegans'.

Frøkjaer-Jensen, C., Davis, M. W., Hopkins, C. E., Newman, B. J., Thummel, J. M., Olesen, S. P., Grunnet, M. and Jorgensen, E. M. (2008) 'Single-copy insertion of transgenes in Caenorhabditis elegans', *Nat Genet*, 40(11), pp. 1375-83.

Goldstein, A. Y. N., Wang, X. and Schwarz, T. L. (2008) 'Axonal transport and the delivery of pre-synaptic components', *Current opinion in neurobiology*, 18(5), pp. 495-503.

Goodwin, P. R. and Juo, P. (2013) 'The Scaffolding Protein SYD-2/Liprin-α Regulates the Mobility and Polarized Distribution of Dense-Core Vesicles in C. elegans Motor Neurons', *PLOS ONE*, 8(1), pp. e54763.

Götz, T. W. B., Puchkov, D., Lysiuk, V., Lützkendorf, J., Nikonenko, A. G., Quentin, C., Lehmann, M., Sigrist, S. J. and Petzoldt, A. G. (2021) 'Rab2 regulates presynaptic precursor vesicle biogenesis at the trans-Golgi', *J Cell Biol*, 220(5).

Hall, D. H. and Hedgecock, E. M. (1991) 'Kinesin-related gene unc-104 is required for axonal transport of synaptic vesicles in C. elegans', *Cell*, 65(5), pp. 837-47.

Hamelin, M., Scott, I. M., Way, J. C. and Culotti, J. G. (1992) 'The mec-7 beta-tubulin gene of Caenorhabditis elegans is expressed primarily in the touch receptor neurons', *Embo j*, 11(8), pp. 2885-93.

Heaton, G. R., Landeck, N., Mamais, A., Nalls, M. A., Nixon-Abell, J., Kumaran, R., Beilina, A., Pellegrini, L., Li, Y., Harvey, K. and Cookson, M. R. (2020) 'Sequential screening nominates the Parkinson's disease associated kinase LRRK2 as a regulator of Clathrin-mediated endocytosis', *Neurobiol Dis*, 141, pp. 104948.

Inoshita, T., Liu, J. Y., Taniguchi, D., Ishii, R., Shiba-Fukushima, K., Hattori, N. and Imai, Y. (2022) 'Parkinson disease-associated Leucine-rich repeat kinase regulates UNC-104-dependent axonal transport of Arl8-positive vesicles in Drosophila', *iScience*, 25(12), pp. 105476.

Iovino, L., Giusti, V., Pischedda, F., Giusto, E., Plotegher, N., Marte, A., Battisti, I., Di Iacovo, A., Marku, A., Piccoli, G., Bandopadhyay, R., Perego, C., Bonifacino, T., Bonanno, G., Roseti, C., Bossi, E., Arrigoni, G., Bubacco, L., Greggio, E., Hilfiker, S. and Civiero, L. (2022) 'Trafficking of the glutamate transporter is impaired in LRRK2-related Parkinson's disease', *Acta Neuropathologica*, 144(1), pp. 81-106.

Janvier, K. and Bonifacino, J. S. (2005) 'Role of the endocytic machinery in the sorting of lysosome-associated membrane proteins', *Molecular biology of the cell*, 16(9), pp. 4231-4242.

Jin, Y. and Garner, C. C. (2008) 'Molecular mechanisms of presynaptic differentiation', *Annual review of cell and developmental biology*, 24, pp. 237-62.

Kalatzis, V., Cherqui, S., Antignac, C. and Gasnier, B. (2001) 'Cystinosin, the protein defective in cystinosis, is a H(+)-driven lysosomal cystine transporter', *Embo j*, 20(21), pp. 5940-9.

785 Ko, J., Na, M., Kim, S., Lee, J. R. and Kim, E. (2003) 'Interaction of the ERC family of RIM-
786 binding proteins with the liprin-alpha family of multidomain proteins', *J Biol Chem,* 278(43),
787 pp. 42377-85.
788 Kraemer, B. C., Zhang, B., Leverenz, J. B., Thomas, J. H., Trojanowski, J. Q. and
789 Schellenberg, G. D. (2003) 'Neurodegeneration and defective neurotransmission in a
790 Caenorhabditis elegans model of tauopathy', *Proc Natl Acad Sci U S A,* 100(17), pp. 9980-5.
791 Kumar, J., Choudhary, B. C., Metpally, R., Zheng, Q., Nonet, M. L., Ramanathan, S.,
792 Klopfenstein, D. R. and Koushika, S. P. (2010) 'The Caenorhabditis elegans Kinesin-3 Motor
793 UNC-104/KIF1A Is Degraded upon Loss of Specific Binding to Cargo', *PLOS Genetics,*
794 6(11), pp. e1001200.
795 Kuwahara, T., Inoue, K., D'Agati, V. D., Fujimoto, T., Eguchi, T., Saha, S., Wolozin, B.,
796 Iwatsubo, T. and Abeliovich, A. (2016) 'LRRK2 and RAB7L1 coordinately regulate axonal
797 morphology and lysosome integrity in diverse cellular contexts', *Scientific reports,* 6, pp.
798 29945-29945.
799 Lanning, N. J., VanOpstall, C., Goodall, M. L., MacKeigan, J. P. and Looyenga, B. D. (2018)
800 'LRRK2 deficiency impairs trans-Golgi to lysosome trafficking and endocytic cargo
801 degradation in human renal proximal tubule epithelial cells', *Am J Physiol Renal Physiol,*
802 315(5), pp. F1465-f1477.
803 Linhart, R., Wong, S. A., Cao, J., Tran, M., Huynh, A., Ardrey, C., Park, J. M., Hsu, C.,
804 Taha, S., Peterson, R., Shea, S., Kurian, J. and Venderova, K. (2014) 'Vacuolar protein
805 sorting 35 (Vps35) rescues locomotor deficits and shortened lifespan in Drosophila
806 expressing a Parkinson's disease mutant of Leucine-Rich Repeat Kinase 2 (LRRK2)', *Mol*
807 *Neurodegener,* 9, pp. 23.
808 Lipton, D. M., Maeder, C. I. and Shen, K. (2018) 'Axonal transport and active zone proteins
809 regulate volume transmitting dopaminergic synapse formation', *bioRxiv*, pp. 284042.
810 Maas, C., Torres, V. I., Altrock, W. D., Leal-Ortiz, S., Wagh, D., Terry-Lorenzo, R. T.,
811 Fejtova, A., Gundelfinger, E. D., Ziv, N. E. and Garner, C. C. (2012) 'Formation of Golgi-
812 derived active zone precursor vesicles', *The Journal of neuroscience : the official journal of*
813 *the Society for Neuroscience,* 32(32), pp. 11095-11108.
814 MacLeod, D. A., Rhinn, H., Kuwahara, T., Zolin, A., Di Paolo, G., McCabe, B. D., Marder,
815 K. S., Honig, L. S., Clark, L. N., Small, S. A. and Abeliovich, A. (2013) 'RAB7L1 interacts
816 with LRRK2 to modify intraneuronal protein sorting and Parkinson's disease risk', *Neuron,*
817 77(3), pp. 425-39.
818 Madero-Pérez, J., Fdez, E., Fernández, B., Lara Ordóñez, A. J., Blanca Ramírez, M., Gómez-
819 Suaga, P., Waschbüsch, D., Lobbestael, E., Baekelandt, V., Nairn, A. C., Ruiz-Martínez, J.,
820 Aiastui, A., López de Munain, A., Lis, P., Comptdaer, T., Taymans, J.-M., Chartier-Harlin,
821 M.-C., Beilina, A., Gonnelli, A., Cookson, M. R., Greggio, E. and Hilfiker, S. (2018)
822 'Parkinson disease-associated mutations in LRRK2 cause centrosomal defects via Rab8a
823 phosphorylation', *Molecular Neurodegeneration,* 13(1), pp. 3.
824 Maeder, C. I., Shen, K. and Hoogenraad, C. C. (2014) 'Axon and dendritic trafficking',
825 *Current Opinion in Neurobiology,* 27, pp. 165-170.
826 Mahoney, T. R., Luo, S. and Nonet, M. L. (2006) 'Analysis of synaptic transmission in
827 Caenorhabditis elegans using an aldicarb-sensitivity assay', *Nat Protoc,* 1(4), pp. 1772-7.
828 Nadiminti, S. S. P. and Koushika, S. P. (2022) 'Imaging Intracellular Trafficking in Neurons
829 of C. elegans', *Methods Mol Biol,* 2431, pp. 499-530.
830 Nakagawa, T., Setou, M., Seog, D.-H., Ogasawara, K., Dohmae, N., Takio, K. and Hirokawa,
831 N. (2000) 'A Novel Motor, KIF13A, Transports Mannose-6-Phosphate Receptor to Plasma
832 Membrane through Direct Interaction with AP-1 Complex', *Cell,* 103(4), pp. 569-581.
833 Nakata, T., Terada, S. and Hirokawa, N. (1998) 'Visualization of the dynamics of synaptic
834 vesicle and plasma membrane proteins in living axons', *J Cell Biol,* 140(3), pp. 659-74.

835   Newell-Litwa, K., Salazar, G., Smith, Y. and Faundez, V. (2009) 'Roles of BLOC-1 and
836   adaptor protein-3 complexes in cargo sorting to synaptic vesicles', *Mol Biol Cell,* 20(5), pp.
837   1441-53.
838   Nonet, M. L., Saifee, O., Zhao, H., Rand, J. B. and Wei, L. (1998) 'Synaptic transmission
839   deficits in Caenorhabditis elegans synaptobrevin mutants', *J Neurosci,* 18(1), pp. 70-80.
840   Nyitrai, H., Wang, S. S. H. and Kaeser, P. S. (2020) 'ELKS1 Captures Rab6-Marked
841   Vesicular Cargo in Presynaptic Nerve Terminals', *Cell Rep,* 31(10), pp. 107712.
842   Okada, Y. and Hirokawa, N. (1999) 'A processive single-headed motor: kinesin superfamily
843   protein KIF1A', *Science,* 283(5405), pp. 1152-7.
844   Pack-Chung, E., Kurshan, P. T., Dickman, D. K. and Schwarz, T. L. (2007) 'A Drosophila
845   kinesin required for synaptic bouton formation and synaptic vesicle transport', *Nature*
846   *Neuroscience,* 10(8), pp. 980-989.
847   Patwardhan, A., Bardin, S., Miserey-Lenkei, S., Larue, L., Goud, B., Raposo, G. and
848   Delevoye, C. (2017) 'Routing of the RAB6 secretory pathway towards the lysosome related
849   organelle of melanocytes'.
850   Piccoli, G. and Volta, M. (2021) 'LRRK2 along the Golgi and lysosome connection: a
851   jamming situation', *Biochem Soc Trans,* 49(5), pp. 2063-2072.
852   Richmond, J. E., Davis, W. S. and Jorgensen, E. M. (1999) 'UNC-13 is required for synaptic
853   vesicle fusion in C. elegans', *Nat Neurosci,* 2(11), pp. 959-64.
854   Rizalar, F. S., Roosen, D. A. and Haucke, V. (2021) 'A Presynaptic Perspective on Transport
855   and Assembly Mechanisms for Synapse Formation', *Neuron,* 109(1), pp. 27-41.
856   Roux, A., Cappello, G., Cartaud, J., Prost, J., Goud, B. and Bassereau, P. (2002) 'A minimal
857   system allowing tubulation with molecular motors pulling on giant liposomes', *Proceedings*
858   *of the National Academy of Sciences,* 99(8), pp. 5394-5399.
859   Sakaguchi-Nakashima, A., Meir, J. Y., Jin, Y., Matsumoto, K. and Hisamoto, N. (2007)
860   'LRK-1, a C. elegans PARK8-related kinase, regulates axonal-dendritic polarity of SV
861   proteins', *Curr Biol,* 17(7), pp. 592-8.
862   Salazar, G., Love, R., Werner, E., Doucette, M. M., Cheng, S., Levey, A. and Faundez, V.
863   (2004) 'The zinc transporter ZnT3 interacts with AP-3 and it is preferentially targeted to a
864   distinct synaptic vesicle subpopulation', *Molecular biology of the cell,* 15(2), pp. 575-587.
865   Schindelin, J., Arganda-Carreras, I., Frise, E., Kaynig, V., Longair, M., Pietzsch, T.,
866   Preibisch, S., Rueden, C., Saalfeld, S., Schmid, B., Tinevez, J.-Y., White, D. J., Hartenstein,
867   V., Eliceiri, K., Tomancak, P. and Cardona, A. (2012) 'Fiji: an open-source platform for
868   biological-image analysis', *Nature Methods,* 9(7), pp. 676-682.
869   Schoppe, J., Schubert, E., Apelbaum, A., Yavavli, E., Birkholz, O., Stephanowitz, H., Han,
870   Y., Perz, A., Hofnagel, O., Liu, F., Piehler, J., Raunser, S. and Ungermann, C. (2021)
871   'Flexible open conformation of the AP-3 complex explains its role in cargo recruitment at the
872   Golgi', *Journal of Biological Chemistry,* 297(5).
873   Shin, H., Wyszynski, M., Huh, K. H., Valtschanoff, J. G., Lee, J. R., Ko, J., Streuli, M.,
874   Weinberg, R. J., Sheng, M. and Kim, E. (2003) 'Association of the kinesin motor KIF1A with
875   the multimodular protein liprin-alpha', *J Biol Chem,* 278(13), pp. 11393-401.
876   Steger, M., Tonelli, F., Ito, G., Davies, P., Trost, M., Vetter, M., Wachter, S., Lorentzen, E.,
877   Duddy, G., Wilson, S., Baptista, M. A., Fiske, B. K., Fell, M. J., Morrow, J. A., Reith, A. D.,
878   Alessi, D. R. and Mann, M. (2016) 'Phosphoproteomics reveals that Parkinson's disease
879   kinase LRRK2 regulates a subset of Rab GTPases', *Elife,* 5.
880   Stucchi, R., Plucińska, G., Hummel, J. J. A., Zahavi, E. E., Guerra San Juan, I., Klykov, O.,
881   Scheltema, R. A., Altelaar, A. F. M. and Hoogenraad, C. C. (2018) 'Regulation of KIF1A-
882   Driven Dense Core Vesicle Transport: Ca(2+)/CaM Controls DCV Binding and Liprin-
883   α/TANC2 Recruits DCVs to Postsynaptic Sites', *Cell Rep,* 24(3), pp. 685-700.

Takamori, S., Holt, M., Stenius, K., Lemke, E. A., Grønborg, M., Riedel, D., Urlaub, H., Schenck, S., Brügger, B., Ringler, P., Müller, S. A., Rammner, B., Gräter, F., Hub, J. S., De Groot, B. L., Mieskes, G., Moriyama, Y., Klingauf, J., Grubmüller, H., Heuser, J., Wieland, F. and Jahn, R. (2006) 'Molecular anatomy of a trafficking organelle', *Cell,* 127(4), pp. 831-46.

Tao-Cheng, J.-H. (2020) 'Immunogold labeling of synaptic vesicle proteins in developing hippocampal neurons', *Molecular Brain,* 13(1), pp. 9.

Tsukita, S. and Ishikawa, H. (1980) 'The movement of membranous organelles in axons. Electron microscopic identification of anterogradely and retrogradely transported organelles', *Journal of Cell Biology,* 84(3), pp. 513-530.

Vilariño-Güell, C., Wider, C., Ross, O. A., Dachsel, J. C., Kachergus, J. M., Lincoln, S. J., Soto-Ortolaza, A. I., Cobb, S. A., Wilhoite, G. J., Bacon, J. A., Behrouz, B., Melrose, H. L., Hentati, E., Puschmann, A., Evans, D. M., Conibear, E., Wasserman, W. W., Aasly, J. O., Burkhard, P. R., Djaldetti, R., Ghika, J., Hentati, F., Krygowska-Wajs, A., Lynch, T., Melamed, E., Rajput, A., Rajput, A. H., Solida, A., Wu, R. M., Uitti, R. J., Wszolek, Z. K., Vingerhoets, F. and Farrer, M. J. (2011) 'VPS35 mutations in Parkinson disease', *Am J Hum Genet,* 89(1), pp. 162-7.

Vukoja, A., Rey, U., Petzoldt, A. G., Ott, C., Vollweiter, D., Quentin, C., Puchkov, D., Reynolds, E., Lehmann, M., Hohensee, S., Rosa, S., Lipowsky, R., Sigrist, S. J. and Haucke, V. (2018) 'Presynaptic Biogenesis Requires Axonal Transport of Lysosome-Related Vesicles', *Neuron,* 99(6), pp. 1216-1232.e7.

Wagner, O. I., Esposito, A., Köhler, B., Chen, C.-W., Shen, C.-P., Wu, G.-H., Butkevich, E., Mandalapu, S., Wenzel, D., Wouters, F. S. and Klopfenstein, D. R. (2009) 'Synaptic scaffolding protein SYD-2 clusters and activates kinesin-3 UNC-104 in C. elegans', *Proceedings of the National Academy of Sciences,* 106(46), pp. 19605-19610.

Wallings, R., Connor-Robson, N. and Wade-Martins, R. (2019) 'LRRK2 interacts with the vacuolar-type H+-ATPase pump a1 subunit to regulate lysosomal function', *Human molecular genetics,* 28(16), pp. 2696-2710.

Weindel, C. G., Bell, S. L., Vail, K. J., West, K. O., Patrick, K. L. and Watson, R. O. (2020) 'LRRK2 maintains mitochondrial homeostasis and regulates innate immune responses to Mycobacterium tuberculosis', *eLife,* 9, pp. e51071.

Xiong, Y., Yuan, C., Chen, R., Dawson, T. M. and Dawson, V. L. (2012) 'ArfGAP1 is a GTPase activating protein for LRRK2: reciprocal regulation of ArfGAP1 by LRRK2', *The Journal of neuroscience : the official journal of the Society for Neuroscience,* 32(11), pp. 3877-3886.

Xuan, Z., Manning, L., Nelson, J., Richmond, J. E., Colón-Ramos, D. A., Shen, K. and Kurshan, P. T. (2017) 'Clarinet (CLA-1), a novel active zone protein required for synaptic vesicle clustering and release', *eLife,* 6, pp. e29276.

Yan, J., Chao, D. L., Toba, S., Koyasako, K., Yasunaga, T., Hirotsune, S. and Shen, K. (2013) 'Kinesin-1 regulates dendrite microtubule polarity in Caenorhabditis elegans', *Elife,* 2, pp. e00133.

Zhao, C., Takita, J., Tanaka, Y., Setou, M., Nakagawa, T., Takeda, S., Yang, H. W., Terada, S., Nakata, T., Takei, Y., Saito, M., Tsuji, S., Hayashi, Y. and Hirokawa, N. (2001) 'Charcot-Marie-Tooth disease type 2A caused by mutation in a microtubule motor KIF1Bbeta', *Cell,* 105(5), pp. 587-97.

Zhao, H. and Nonet, M. L. (2001) 'A Conserved Mechanism of Synaptogyrin Localization', *Molecular biology of the cell,* vol. 12 (2001)(8), pp. 2275-89.

Zhen, M. and Jin, Y. (1999) 'The liprin protein SYD-2 regulates the differentiation of presynaptic termini in C. elegans', *Nature,* 401(6751), pp. 371-375.

933   Zheng, Q., Ahlawat, S., Schaefer, A., Mahoney, T., Koushika, S. P. and Nonet, M. L. (2014)
934   'The Vesicle Protein SAM-4 Regulates the Processivity of Synaptic Vesicle Transport', *PLOS*
935   *Genetics*, 10(10), pp. e1004644.
936   Zimprich, A., Benet-Pagès, A., Struhal, W., Graf, E., Eck, S. H., Offman, M. N.,
937   Haubenberger, D., Spielberger, S., Schulte, E. C., Lichtner, P., Rossle, S. C., Klopp, N.,
938   Wolf, E., Seppi, K., Pirker, W., Presslauer, S., Mollenhauer, B., Katzenschlager, R., Foki, T.,
939   Hotzy, C., Reinthaler, E., Harutyunyan, A., Kralovics, R., Peters, A., Zimprich, F., Brücke,
940   T., Poewe, W., Auff, E., Trenkwalder, C., Rost, B., Ransmayr, G., Winkelmann, J.,
941   Meitinger, T. and Strom, T. M. (2011) 'A mutation in VPS35, encoding a subunit of the
942   retromer complex, causes late-onset Parkinson disease', *Am J Hum Genet*, 89(1), pp. 168-75.
943

Figure legends

Figure 1: Synaptic vesicle proteins travel with lysosomal proteins in heterogenous carriers

(A) Quantitation of co-transport of different combinations of synaptic vesicle proteins and lysosomal proteins from kymograph analysis of dual color imaging. The number of animals per genotype (N) ≥ 10. Number of vesicles analyzed (n) > 600.

(B) Quantitation of fraction of different lysosomal proteins co-transporting different synaptic vesicle proteins from kymograph analysis of dual color imaging. N ≥ 10; n > 100.

(C) Quantitation of fraction of CTNS-1-labelled compartments moving in the anterograde and retrograde direction in different mutants. N ≥ 9 per genotype; the number of CTNS-1-labelled compartments ≥ 20.

(D) Quantitation of co-transport of CTNS-1::mCherry and mNeonGreen::RAB-7 in WT animals from sequential dual color imaging at 1.3 fps. CTNS-1 with RAB-7 indicates the fraction of CTNS-1-labelled compartments co-transporting RAB-7. RAB-7 with CTNS-1 indicates the fraction of RAB-7-labelled compartments co-transporting CTNS-1. N ≥ 15 animals; n > 450.

(E) Schematic showing the PLM neuron. Red boxes highlight the regions of imaging. The arrow shows the anterograde direction of vesicle motion.

(F) GFP::RAB-3, SNG-1::GFP, CTNS-1::mCherry, and RAB-7::mScarlet in the cell body, process and synapses of wildtype PLM neurons. Scale bar: 10 μm.

Figure 2: LRK-1 and AP-3 act in parallel and through SYD-2 to regulate lysosomal protein trafficking.

(A) Quantitation of co-transport of SNG-1::eGFP and mCherry::RAB-3 in WT, *lrk-1(km17)*, and *apb-3(ok429)* from kymograph analysis of sequential dual color imaging at 1.3 frames

969   per second (fps). # P-value ≤ 0.05 (One-Way ANOVA with Tukey's post-hoc test, all

970   comparisons to WT); ns: not significant; Number of animals (N) ≥ 15 per genotype; Number

971   of vesicles analyzed per genotype (n) > 800.

972   (B) Quantitation of fraction of SNG-1-carrying vesicles co-transporting CTNS-1 in WT, *lrk-*

973   *1(km17)*, *lrk-1(km41)*, *apb-3(ok429)* and *lrk-1(km17) apb-3(ok429)*, from kymograph

974   analysis of sequential dual color imaging at 1.3 fps. # P-value ≤ 0.05 (Mann–Whitney Test);

975   N ≥ 15 per genotype; n > 500.

976   (C) Quantitation of fraction of SNG-1-carrying vesicles co-transporting RAB-7 from WT,

977   *lrk-1(km17)*, *apb-3(ok429)* and *lrk-1(km17) apb-3(ok429)*, kymograph analysis of dual color

978   imaging. # P-value ≤ 0.05 (One-Way ANOVA with Tukey's post-hoc test, all comparisons to

979   WT); ns: not significant; N ≥ 20 per genotype; n > 800.

980   (D) CTNS-1::mCherry in the cell body, process, and synapses of PLM neurons of WT, *lrk-*

981   *1(km17)*, *apb-3(ok429)*, and *lrk-1(km17) apb-3(ok429)*. Scale bar: 10 μm. Red arrows point

982   to some CTNS-1-labelled compartments.

983   (E) mScarlet::RAB-7 in the cell body, process, and synapses of PLM neurons of WT, *lrk-*

984   *1(km17)*, *apb-3(ok429)*, and *lrk-1(km17) apb-3(ok429)*. Scale bar: 10 μm. Red arrows point

985   to some RAB-7-labelled compartments.

986   (F) LMP-1::mNeonGreen in the cell body, process, and synapses of PLM neurons of WT,

987   *lrk-1(km17)*, *apb-3(ok429)*, and *lrk-1(km17) apb-3(ok429)*. Scale bar: 10 μm. Red arrows

988   point to some RAB-7-labelled compartments.

989   (G) Images showing APB-3::GFP puncta in the head ganglion cell bodies of WT, *lrk-*

990   *1(km17)*, and *syd-2(ok217)*. Scale bar: 10 μm. Red boxes highlight the regions of insets with

991   cell bodies from images showing APB-3::GFP in (i) WT, (ii) *lrk-1*, and (iii) *syd-2*.

992   (H) Quantitation of the number of APB-3::GFP puncta per cell body in WT, *lrk-1*(*km17*), and

993   *syd-2*(*ok217*). # P-value ≤ 0.05 (Mann–Whitney Test); ns: not significant; N > 10 animals; n

994   > 75 cell bodies.

995   (I) Quantitation of intensity of APB-3::GFP puncta in cell bodies of WT, *lrk-1*(*km17*), and

996   *syd-2*(*ok217*). The ratio of the intensity of APB-3::GFP puncta to cytosolic intensity in the

997   cell body is plotted. # P-value ≤ 0.05 (Mann–Whitney Test); ns: not significant; N > 10

998   animals; n > 75 cell bodies.

999   (J) Quantitation of average size of APB-3::GFP puncta per cell body in WT, *lrk-1*(*km17*), and

1000   *syd-2*(*ok217*). # P-value ≤ 0.05 (Mann–Whitney Test); ns: not significant; N > 10 animals; n

1001   > 75 cell bodies.

1002

1003   **Figure 3: SV-lysosomes in *lrk-1* and *apb-3* mutants are dependent on UNC-104**

1004   (A) Schematic showing the PLM neuron. Red boxes highlight the regions of imaging.

1005   (B) SNG-1::GFP in the cell body, process, and synapses of PLM neurons showing

1006   dependence on UNC-104 in *lrk-1*(*km17*) and *apb-3*(*ok429*) mutants and their doubles with

1007   *unc-104*(*e1265tb120*). Scale bar: 10 μm.

1008   (C) CTNS-1::mCherry in the cell body, process, and synapses of PLM neurons showing

1009   dependence on UNC-104 in *lrk-1*(*km17*) and *apb-3*(*ok429*) mutants and their doubles with

1010   *unc-104*(*e1265tb120*). Red arrows highlight fainter CTNS-1 puncta. Scale bar: 10 μm.

1011   (D) Quantitation of co-transport of SNG-1 and CTNS-1 in *unc-104*(*e1265tb120*), *lrk-*

1012   *1*(*km17*); *unc-104*, and *apb-3*(*ok429*); *unc-104* from kymograph analysis of sequential dual

1013   color imaging done at 1.3 fps. #P-value ≤ 0.05 (Mann–Whitney Test, all comparisons to

1014   WT); ns: not significant; Number of animals (N) ≥ 18 per genotype; Number of vesicles (n) >

1015   1200.

1016

Figure 4: Distribution of SV-lysosomal compartments depends on UNC-104

(A) Quantitation of co-transport of SNG-1 and CTNS-1 in *syd-2* mutants and their doubles with *lrk-1(km17)* and *apb-3(ok429)*, from kymograph analysis of dual color imaging. *ok217* refers to the null allele of *syd-2*, *syd-2(ok217)*; while *ju37* refers to the *syd-2(ju37)* allele. #P-value ≤ 0.05 (Mann–Whitney Test, all comparisons to WT); ns: not significant; Number of animals (N) ≥ 18 per genotype; Number of vesicles (n) > 750. Values for *lrk-1* and *apb-3* single mutants are the same as those in Fig. 2B.

(B) Quantitation of co-transport of SNG-1 and RAB-7 in *syd-2(ok217)* and its doubles with *lrk-1(km17)* and *apb-3(ok429)*, from kymograph analysis of dual color sequential imaging at 1.3 fps. P-value > 0.05 (One-Way ANOVA with Tukey's post-hoc test); ns: not significant; N ≥ 19 per genotype; n > 700. Values for *lrk-1* and *apb-3* single mutants are the same as those in Fig. 2C.

(C) CTNS-1::mCherry in the cell body, process, and synapses of PLM neurons of *syd-2(ok217)* mutant and its doubles with *lrk-1(km17)* and *apb-3(ok429)*. Red arrows highlight some CTNS-1-carrying compartments, some fainter. Scale bar: 10 μm.

(D) mScarlet::RAB-7 in the cell body, process, and synapses of PLM neurons of *syd-2(ok217)* mutant and its doubles with *lrk-1(km17)* and *apb-3(ok429)*. Red arrows highlight some RAB-7-carrying compartments, some fainter. Scale bar: 10 μm.

(E) CTNS-1::mCherry in the cell body, process, and synapses of PLM neurons of *syd-2(ju37)* mutant and its doubles with *lrk-1(km17)* and *apb-3(ok429)*. Red arrows highlight some CTNS-1-carrying compartments, some fainter. Scale bar: 10 μm. Imaged at 100×.

(F) LMP-1::mNeonGreen in the cell body, process, and synapse of PLM neurons of *syd-2(ok217)* mutant and its doubles with *lrk-1(km17)* and *apb-3(ok429)*. Red arrows indicate LMP-1-carrying compartments. Scale bar: 10 μm.

1041　(G) Quantitation of co-transport of SNB-1 and RAB-3, in *syd-2(ok217)*, from simultaneous

1042　dual color imaging at 3 frames per second (fps). # P-value ≤ 0.05 (One-Way ANOVA with

1043　Tukey's post-hoc test); N > 20.

1044　(H) Quantitation of co-transport of SNG-1 and RAB-3, in *syd-2(ok217)*, from sequential dual

1045　color imaging at 1.3 fps. P-value > 0.05 (One-Way ANOVA with Tukey's post-hoc test); ns:

1046　not significant; N > 15.

1047

1048　**Figure 5: SYD-2 is required for UNC-104 dependent of SVp carriers**

1049　(A) Schematic of the PLM neuron. The red box highlights the region of imaging.

1050　(B) SNG-1::GFP in the cell body, process and synapses of PLM neurons of *syd-2(ok217)* and

1051　*unc-104(e1265tb120)*, and their doubles with *lrk-1(km17)* and *apb-3(ok429)*. Scale bar: 10

1052　μm.

1053　(C) CTNS-1::mCherry in the cell body, process and synapses of PLM neurons of *syd-*

1054　*2(ok217)* and *unc-104(e1265tb120)*, and their doubles with *apb-3(ok429)*. Scale bar: 10 μm.

1055　(D) Quantitation of co-transport of SNG-1 and CTNS-1 in WT, *unc-104(e1265tb120)*, *syd-*

1056　*2(ok217)*, and *unc-104*; *syd-2* from kymograph analysis of sequential dual color imaging at

1057　1.3 fps. P-value > 0.05 (Mann–Whitney Test, all comparisons to WT); ns: not significant;

1058　Number of animals (N) > 20 for *unc-104*; *syd-2*; Number of vesicles (n) >1000.

1059

1060　**Figure 6: SYD-2 and the AP-1 complex together regulate the polarized distribution of**

1061　**SVps to axons**

1062　(A) Schematic of the ASI chemosensory neuron. Red box highlights the region of imaging.

1063　(B) SNB-1::GFP in the dendrite of the ASI neuron of WT and two alleles of *syd-2* and their

1064　doubles with *lrk-1(km17)* and *apb-3(ok429)*. *ok217* represents *syd-2(ok217)* allele. *ju37*

1065　represents *syd-2(ju37)* allele. *unc-101(m1)* is a substitution mutation in the μ chain of the AP-

1066   1 complex causing a premature stop. Red arrows point to the SNB-1::GFP signal at the

1067   dendrite tip. Scale bar: 20 μm. Number of animals (N) > 6 per all single mutant genotypes; N

1068   > 20 for all double mutant genotypes.

1069   (C) CTNS-1::mCherry in the dendrite of the ASI neurons of WT, *syd-2(ok217)*, *lrk-1(km17)*,

1070   *apb-3(ok429)*, *unc-101(m1)*, and *unc-101(m1)*; *syd-2(ok217)*. Red arrows point to CTNS-1

1071   compartments in the dendrite. Scale bar: 20 μm. N > 20 per genotype.

1072   (D) Density (number of CTNS-1 puncta per 10 μm in the ASI dendrite) of CTNS-1 in the

1073   ASI dendrite. # P-values ≤ 0.05 (Mann–Whitney Test, black comparisons against WT and

1074   blue comparisons against *lrk-1*); N > 20 for each genotype.

1075   (E) Schematic of *C. elegans* head showing the pharynx (red) and the head ganglion cell

1076   bodies (yellow).

1077   (F) Images showing UNC-101::GFP puncta in the head ganglion cell bodies of WT and *syd-*

1078   *2(ok217)*. Scale bar: 10 μm. The red boxes highlight the regions of insets with cell bodies

1079   from images showing UNC-101::GFP in (i) WT and (ii) *syd-2*.

1080   (G) Quantitation of intensity of UNC-101::GFP puncta in the head ganglion cell bodies in

1081   WT and *syd-2(ok217)*. The ratio of the intensity of UNC-101::GFP puncta to cytosolic

1082   intensity in the cell body is plotted. # P-value ≤ 0.05 (One-Way ANOVA with Tukey's post-

1083   hoc test); N > 5 animals; n > 25 cell bodies.

1084   (H) Quantitation of average size of UNC-101::GFP puncta per cell body in WT and *syd-*

1085   *2(ok217)*. # P-value ≤ 0.05 (Mann–Whitney Test); N > 5 animals; n > 25 cell bodies.

1086   (I) Images showing UNC-101::GFP puncta in the cell bodies of the ventral nerve cord

1087   neurons in WT and *syd-2(ok217)*. Scale bar: 10 μm. The red boxes highlight the regions of

1088   insets with cell bodies from images showing UNC-101::GFP in (i) WT and (ii) *syd-2*.

1089   (J) Quantitation of intensity of UNC-101::GFP puncta in the cell bodies of the ventral nerve

1090   cord in WT and *syd-2(ok217)*. The ratio of the intensity of UNC-101::GFP puncta to

1091   cytosolic intensity in the cell body is plotted. # P-value ≤ 0.05 (Mann–Whitney test); N > 5

1092   animals; n > 10 cell bodies.

1093

1094

1095 **Supplementary Figure Legends**

1096 **Supplementary Figure 1:**

1097 (A) Schematic of the PLM neuron. The red box highlights the region of imaging in the

1098 proximal major neuronal process. The arrow indicates the direction of anterograde motion,

1099 away from the cell body into the neuronal process.

1100 (B) Kymographs from dual-color imaging of RAB-3 with MAN-II in WT, imaged

1101 simultaneously at 3 frames per second (fps). Green traces indicate moving RAB-3 vesicles.

1102 Scale bars x-axis: 5 μm, y-axis: 30 s.

1103 (C) Kymographs from dual-color imaging of SNB-1 with CTNS-1 in WT, imaged

1104 sequentially at 1.3 fps. Green traces indicate moving SNB-1 vesicles, yellow traces indicate

1105 moving vesicles co-transporting SNB-1 and CTNS-1, and red traces indicate moving CTNS-

1106 1 vesicles. Scale bars x-axis: 5 μm, y-axis: 30 s.

1107 (D) Kymographs from dual-color imaging of RAB-3 with CTNS-1, imaged simultaneously at

1108 3 fps. Green traces indicate moving RAB-3 vesicles, yellow traces indicate moving vesicles

1109 co-transporting RAB-3 and CTNS-1, and red traces indicate moving CTNS-1 vesicles. Scale

1110 bars x-axis: 5 μm, y-axis: 10 s.

1111 (E) Kymographs from dual-color imaging of mNeonGreen::RAB-7 with CTNS-1::mCherry,

1112 imaged sequentially at 1.3 fps. Green traces indicate moving RAB-7 vesicles, yellow traces

1113 indicate moving vesicles co-transporting RAB-7 and CTNS-1, and red traces indicate moving

1114 CTNS-1 vesicles. Scale bars x-axis: 5 μm, y-axis: 30 s.

1115 (F) Kymographs from dual-color imaging of SNB-1 with RAB-3, imaged simultaneously at 3

1116 fps. Green traces indicate moving SNB-1 vesicles, yellow traces indicate moving vesicles co-

1117 transporting SNB-1 and RAB-3, and red traces indicate moving RAB-3 vesicles. Scale bars

1118 x-axis: 5 μm, y-axis: 10 s.

1119   (G) Kymographs from dual-color imaging of SNG-1 with RAB-3, imaged sequentially at 1.3

1120   fps. Green traces indicate moving SNG-1 vesicles, yellow traces indicate moving vesicles co-

1121   transporting SNG-1 and RAB-3, and red traces indicate moving RAB-3 vesicles. Scale bars

1122   x-axis: 5 μm, y-axis: 30 s.

1123   (H) Penetrance for the number of animals in which CTNS-1 localizes up to 25 μm of the

1124   PLM neuronal process away from the cell body. Numbers inside the bars indicate the number

1125   of animals per genotype. Numbers above the bars indicate the penetrance values. For bar

1126   graphs with very little height, the lower number indicates the number of animals for that

1127   genotype while the number above indicates the penetrance value.

1128   (I) Penetrance for the number of animals in which RAB-7 localizes up to 25 μm of the PLM

1129   neuronal process away from the cell body. Numbers inside the bars indicate the number of

1130   animals per genotype. Numbers above the bars indicate the penetrance values.

1131   (J) and (K) Penetrance for the number of animals in which LMP-1 localizes up to 25 μm and

1132   50 μm, respectively, of the PLM neuronal process away from the cell body. Numbers inside

1133   the bars indicate the number of animals per genotype. Numbers above the bars indicate the

1134   penetrance values. For bar graphs with very little height, the lower number indicates the

1135   number of animals for that genotype while the number above indicates the penetrance value.

1136

1137   **Supplementary Figure 2:**

1138   (A) Kymographs from sequential dual-color imaging of SNG-1 and CTNS-1 at 1.3 fps in

1139   WT, *lrk-1(km17)*, and *apb-3(ok429)*. Green traces indicate moving SNG-1-carrying vesicles,

1140   yellow traces indicate moving vesicles co-transporting SNG-1 and CTNS-1, and red traces

1141   indicate moving CTNS-1-carrying vesicles. Scale bar x-axis: 5 μm and y-axis: 30 s.

1142   (B) Quantitation of fraction of CTNS-1 co-transporting SNG-1 from kymograph analysis of

1143   dual color imaging. [#]P-values ≤ 0.05 (Mann–Whitney Test, all comparisons to WT); ns: not

1144   significant; Number of animals per genotype (N) ≥ 20; Number of vesicles (n) > 400.

1145   (C) Kymographs from sequential dual-color imaging of SNG-1 and RAB-7 at 1.3 fps in WT,

1146   *lrk-1*(*km17*), and *apb-3*(*ok429*). Green traces indicate moving SNG-1-carrying vesicles,

1147   yellow traces indicate moving vesicles co-transporting SNG-1 and RAB-7, and red traces

1148   indicate moving RAB-7-carrying vesicles. Scale bar x-axis: 5 μm and y-axis: 30 s.

1149   (D) Quantitation of fraction of RAB-7 co-transporting SNG-1 from kymograph analysis of

1150   dual color imaging. # P-values ≤ 0.05 (Mann–Whitney Test, all comparisons to WT); ns: not

1151   significant; N ≥ 20 per genotype; n > 400.

1152   (E) Quantitation of co-transport of SNB-1 and CTNS-1 in WT, *lrk-1*(*km17*), and *apb-*

1153   *3*(*ok429*) from kymograph analysis of dual color imaging. P-values > 0.05 (One-Way

1154   ANOVA with Tukey's post-hoc test, all comparisons to WT); ns: not significant; N ≥ 15 per

1155   genotype; n > 400.

1156   (F) Quantitation of co-transport of RAB-3 and CTNS-1 in WT, *lrk-1*(*km17*), and *apb-*

1157   *3*(*ok429*) from kymograph analysis of simultaneous dual color imaging at 3 fps. # P-values ≤

1158   0.05 (Mann–Whitney Test, all comparisons to WT); ns: not significant; N = 5 per genotype; n

1159   > 500.

1160   (G) Percentages of cell bodies of WT, *lrk-1*, and *syd-2* with APB-3::GFP puncta. N > 10 per

1161   genotype; n > 75 cell bodies.

1162

1163   **Supplementary Figure 3:**

1164   (A) GFP::RAB-3 in the cell body, process, and synapses of PLM neurons showing

1165   dependence on UNC-104 in *lrk-1*(*km17*), *apb-3*(*ok429*), and *syd-2*(*ok217*)mutants, and their

1166   doubles with *unc-104*(*e1265tb120*). Scale bar: 10 μm.

1167   (B) Quantitation of the number of CTNS-1-labelled compartments per 10 μm of the PLM

1168   major neurite proximal to the cell body in WT, *unc-104*(*e1265tb120*), and *syd-2*(*ok217*). # P-

1169   values ≤ 0.05 (Mann–Whitney Test, all comparisons to WT); ns: not significant; Number of

1170   animals (N) ≥ 20 per genotype; Number of CTNS-1-labelled compartments (n) ≥ 70.

1171   (C) Quantitation of co-transport of SNB-1 and CTNS-1 in WT and *syd-2*(*ok217*), from

1172   kymograph analysis of sequential dual color imaging at 1.3 fps. P-value > 0.05 (Mann–

1173   Whitney Test); ns: not significant; N > 15 per genotype; n > 750 vesicles.

1174   (D) Quantitation of co-transport of RAB-3 and CTNS-1, in WT and *syd-2*(*ok217*), from

1175   kymograph analysis of simultaneous dual color imaging at 3 fps. P-value > 0.05 (Mann–

1176   Whitney Test); ns: not significant; N = 5; n > 500 vesicles.

1177

1178   **Supplementary Figure 4:**

1179   (A) Quantitation of fraction of EBP-2::GFP comets moving in either anterograde or

1180   retrograde directions in both the axon and the anterior dendrite of WT and *syd-2*(*ok217*);

1181   Number of animals (N) > 8 for each genotype; Number of comets analyzed (n) > 150.

1182   (B) ODR-1::GFP in the dendrite and axon of the AWC neuron. Red arrow points to the ODR-

1183   1::GFP signal in the AWC axon in *syd-2*(*ok217*), *apb-3*(*ok429*), and *unc-101*(*m1*). Scale bar:

1184   20 μm.

1185   (C) Quantitation of sizes of moving RAB-3 containing SVp carriers in WT, *syd-2*(*ok217*),

1186   *unc-101*(*m1*), and *unc-101*; *syd-2*. The x-axis depicts the length (in μm) of moving RAB-3

1187   carrying SVp carriers. The y-axis depicts the percentage of moving RAB-3 carrying SVp

1188   carriers of various lengths. Number of animals (N) ≥ 9 per genotype; Number of vesicles (n)

1189   > 400.

1190   (D) Quantitation of the number of UNC-101::GFP puncta per cell body in WT and *syd-*

1191   *2*(*ok217*). P-value > 0.05 (Mann–Whitney Test); N > 5 animals; n > 25 cell bodies.

1192   (E) Images showing UNC-101::GFP puncta in the cell bodies of the ventral nerve cord

1193   neurons in WT and *syd-2(ju37)*. Scale bar: 10 μm.

1194   (F) Quantitation of the average size of UNC-101::GFP puncta per cell body in WT and *syd-*

1195   *2(ju37)*. P-value < 0.05 (Mann–Whitney Test); ns: not significant; N > 5 animals; n > 25 cell

1196   bodies.

1197   (G) Quantitation of intensity of UNC-101::GFP puncta in the cell bodies of the ventral nerve

1198   cord in WT and *syd-2(ju37)*. The ratio of the intensity of UNC-101::GFP puncta to cytosolic

1199   intensity in the cell body is plotted. P-value < 0.05 (Mann–Whitney test); ns: not significant;

1200   N > 5 animals; n > 10 cell bodies.

1201

1202 **List of supplementary movies and legends**

1203 **Supplementary movie 1: CTNS-1 and SNG-1 in WT**

1204 SNG-1::GFP and CTNS-1::mCherry in the PLM neuronal process. Imaged sequentially at 1.3

1205 frames per second (fps), playback at 20 fps. Genotype: wildtype. Cell body on the right.

1206

1207 **Supplementary Movie 2: RAB-7 and SNG-1 in WT**

1208 SNG-1::GFP and mScarlet::RAB-7 in the PLM neuronal process. Imaged sequentially at 1.3

1209 frames per second (fps), playback at 20 fps. Genotype: wildtype. Cell body on the right.

1210

1211 **Supplementary Movie 3: CTNS-1 and SNG-1 in *lrk-1***

1212 SNG-1::GFP and CTNS-1::mCherry in the PLM neuronal process. Imaged sequentially at 1.3

1213 frames per second (fps), playback at 20 fps. Genotype: *lrk-1*(*km17*). Cell body on the right.

1214

1215 **Supplementary Movie 4: CTNS-1 and SNG-1 in *apb-3***

1216 SNG-1::GFP and CTNS-1::mCherry in the PLM neuronal process. Imaged sequentially at 1.3

1217 frames per second (fps), playback at 20 fps. Genotype: *apb-3*(*ok429*). Cell body on the right.

1218

1219 **Supplementary Movie 5: RAB-7 and SNG-1 in *lrk-1***

1220 SNG-1::GFP and mScarlet::RAB-7 in the PLM neuronal process. Imaged sequentially at 1.3

1221 frames per second (fps), playback at 20 fps. Genotype: *lrk-1*(*km17*). Cell body on the right.

1222

1223 **Supplementary Movie 6: CTNS-1 and SNG-1 in *unc-104***

1224 SNG-1::GFP and CTNS-1::mCherry in the PLM neuronal process. Imaged sequentially at 1.3

1225 frames per second (fps), playback at 20 fps. Genotype: *unc-104*(*e1265tb120*). Cell body on

1226 the right.

1227

1228 **Supplementary Movie 7: CTNS-1 and SNG-1 in *syd-2***

1229 SNG-1::GFP and CTNS-1::mCherry in the PLM neuronal process. Imaged sequentially at 1.3

1230 frames per second (fps), playback at 20 fps. Genotype: *syd-2(ok217)*. Cell body on the right.
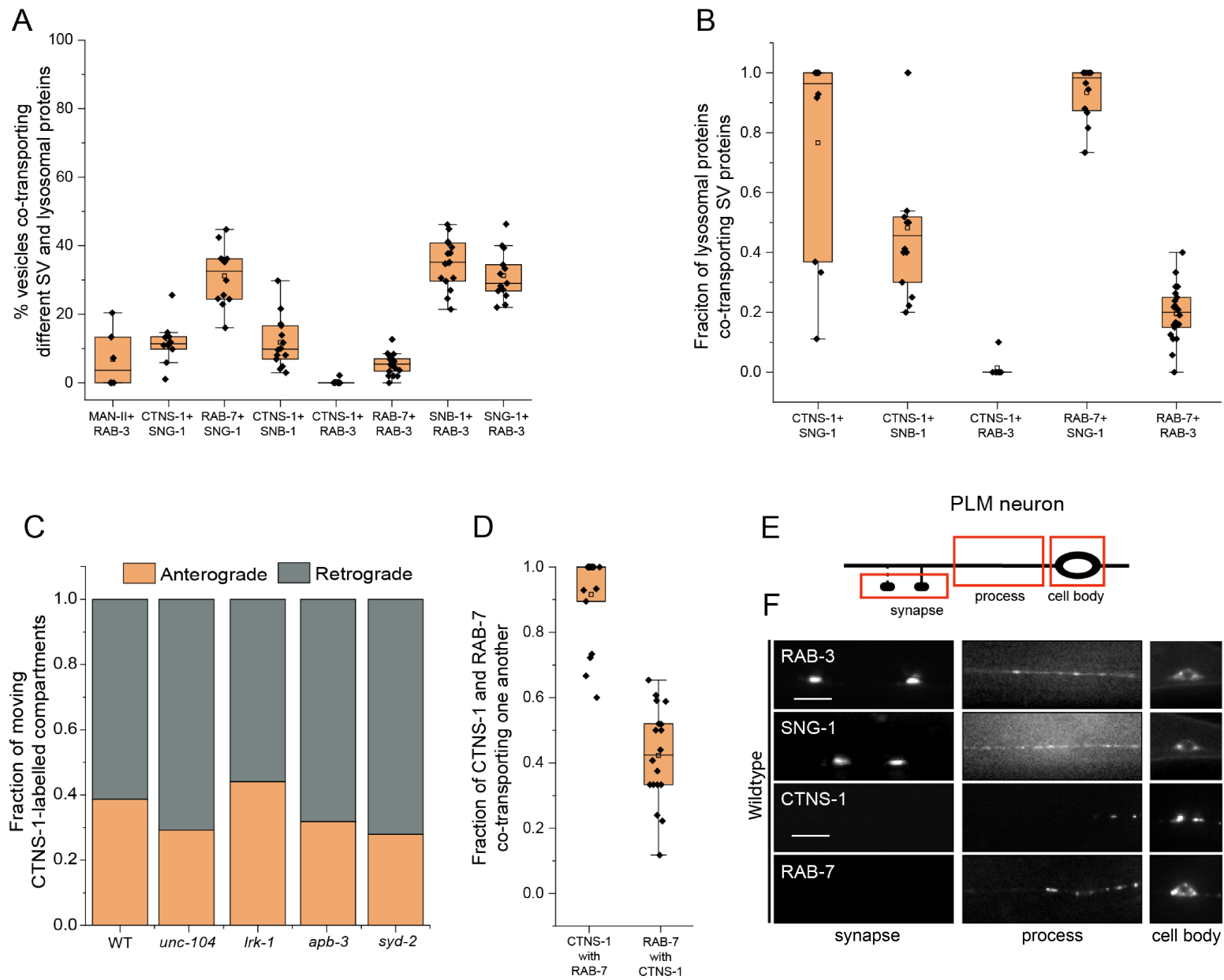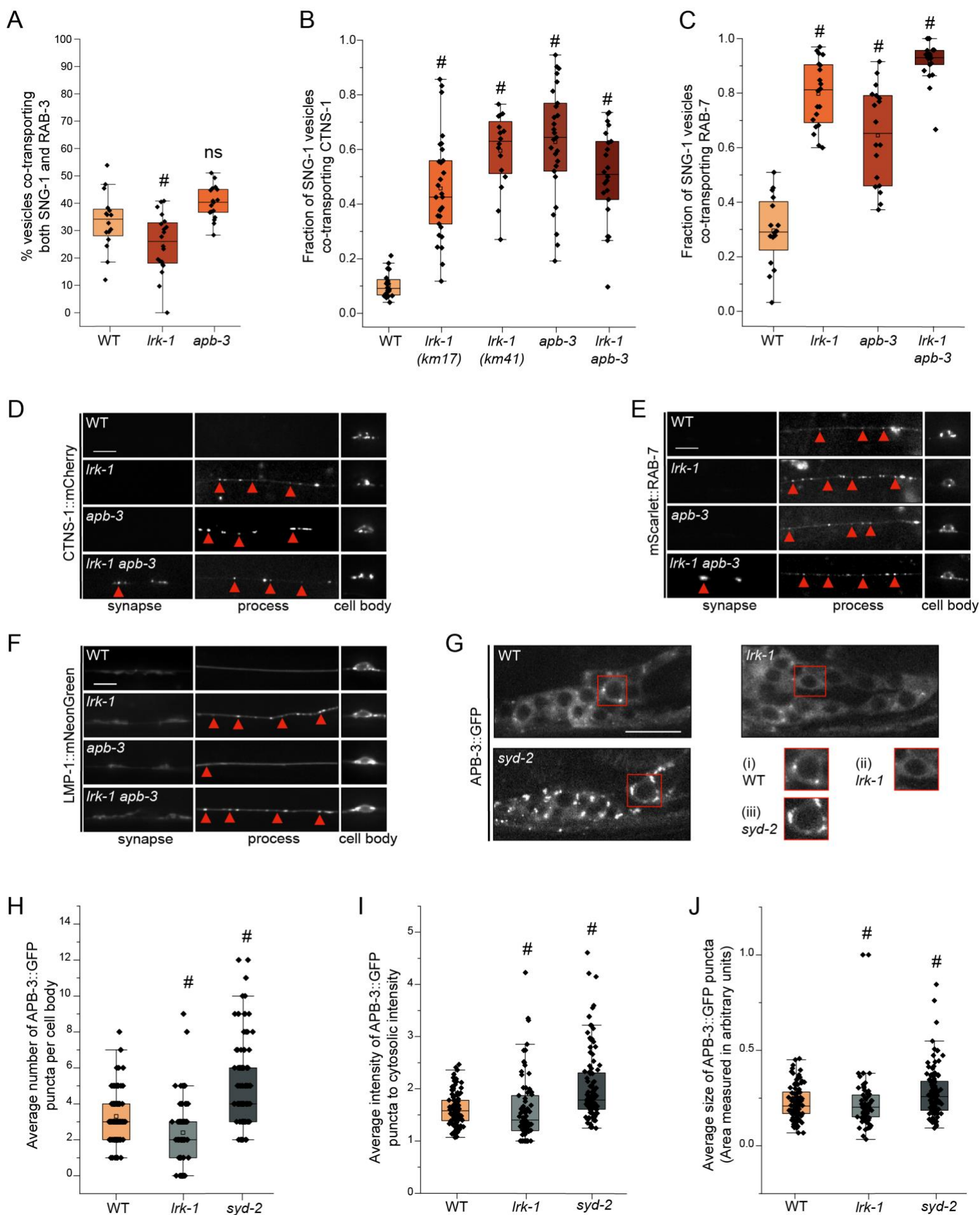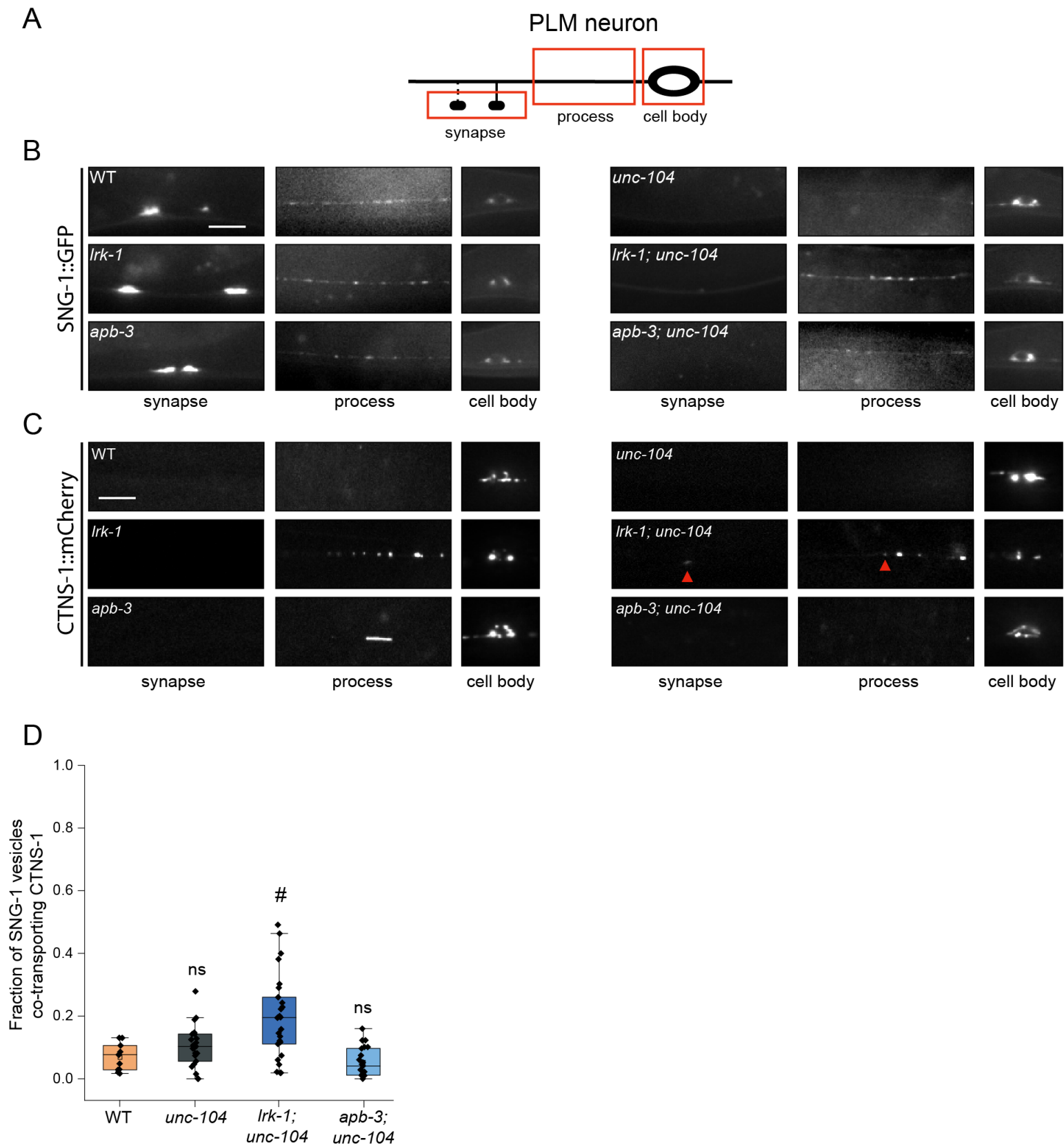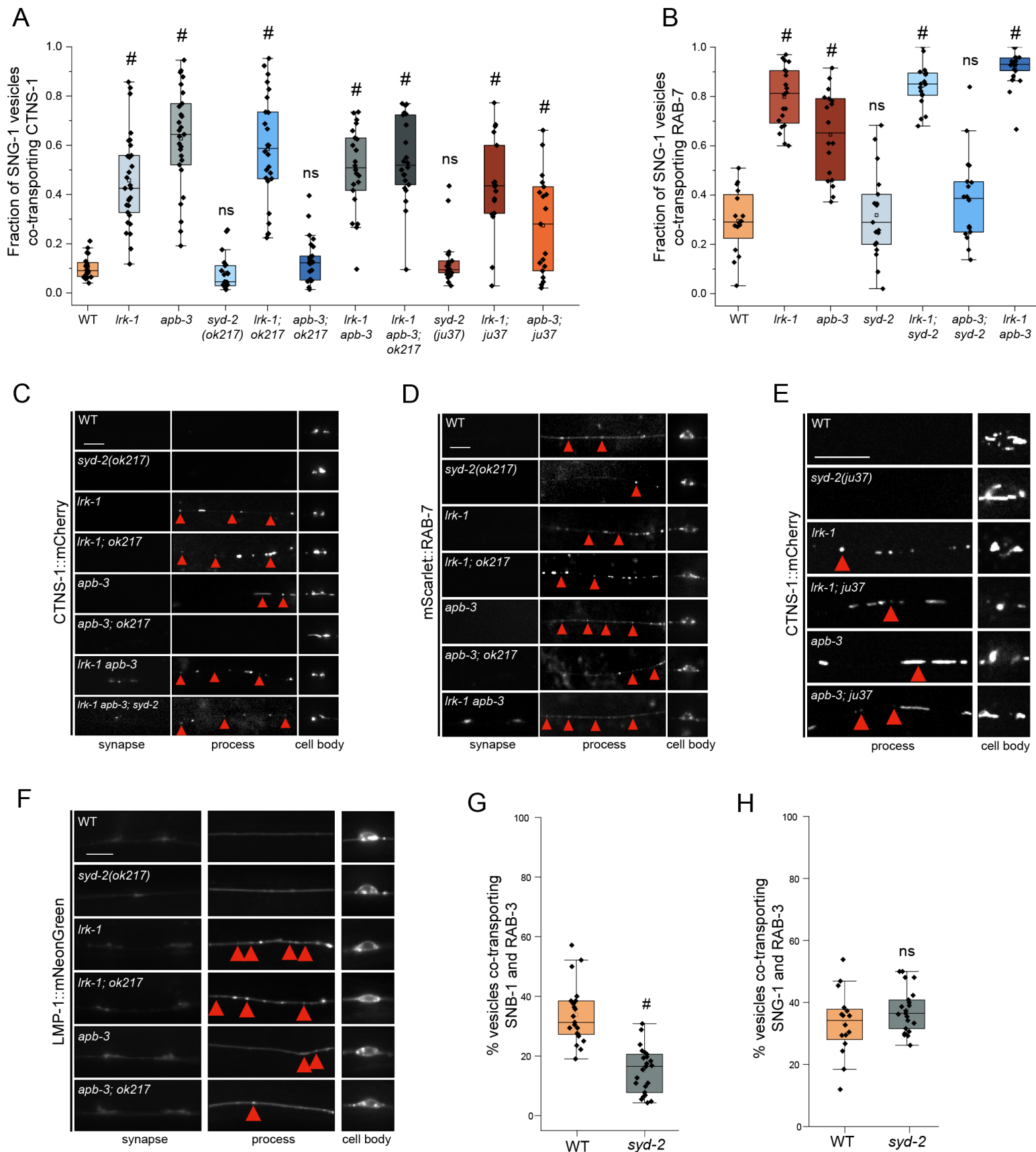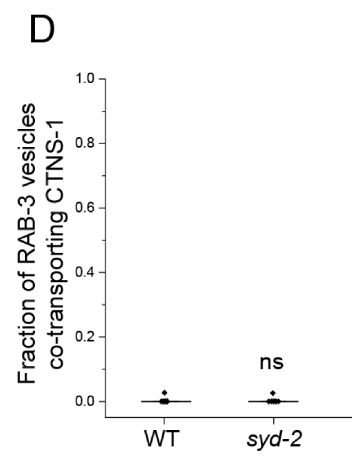
Figure 1

Figure 2

Figure 3

Figure 4
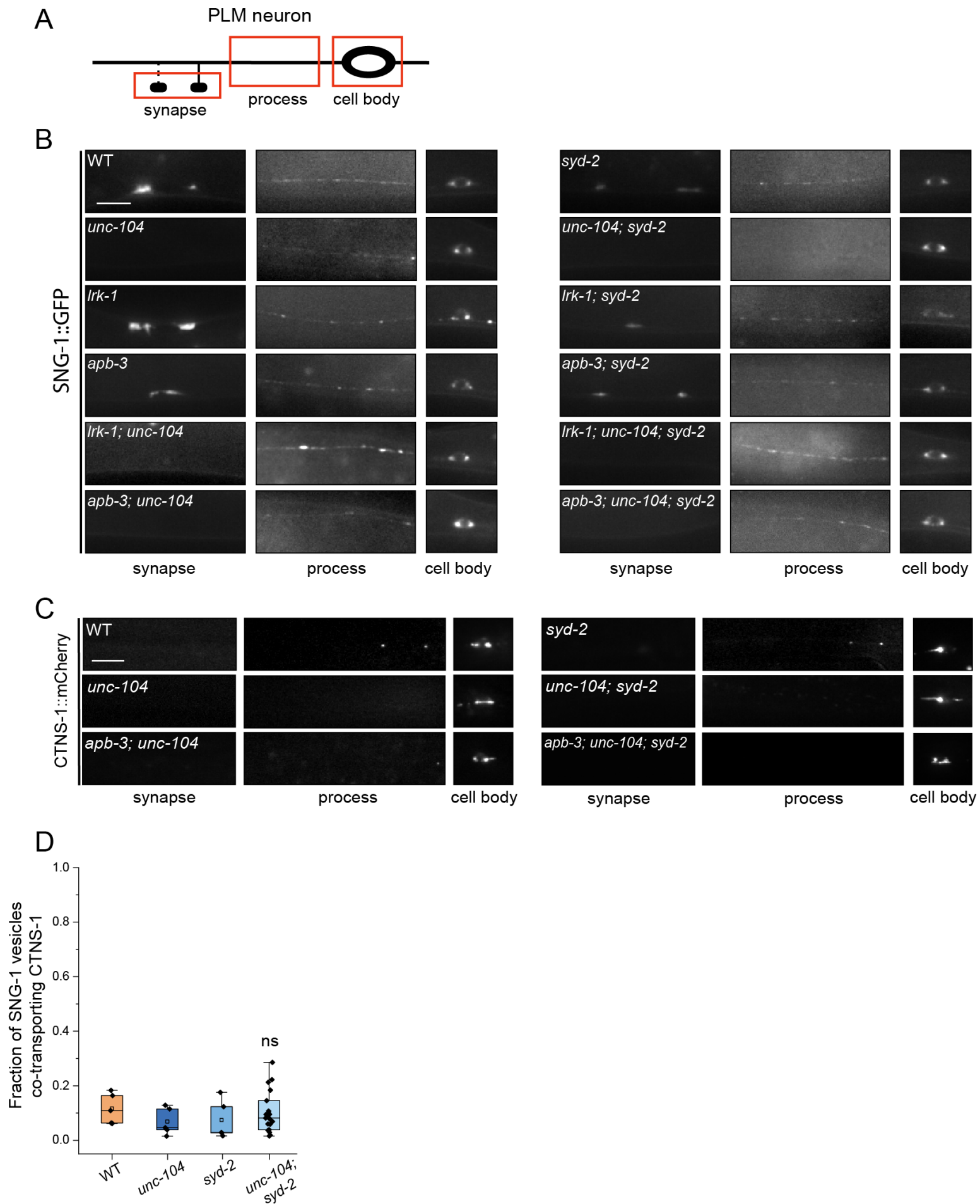
Figure 5
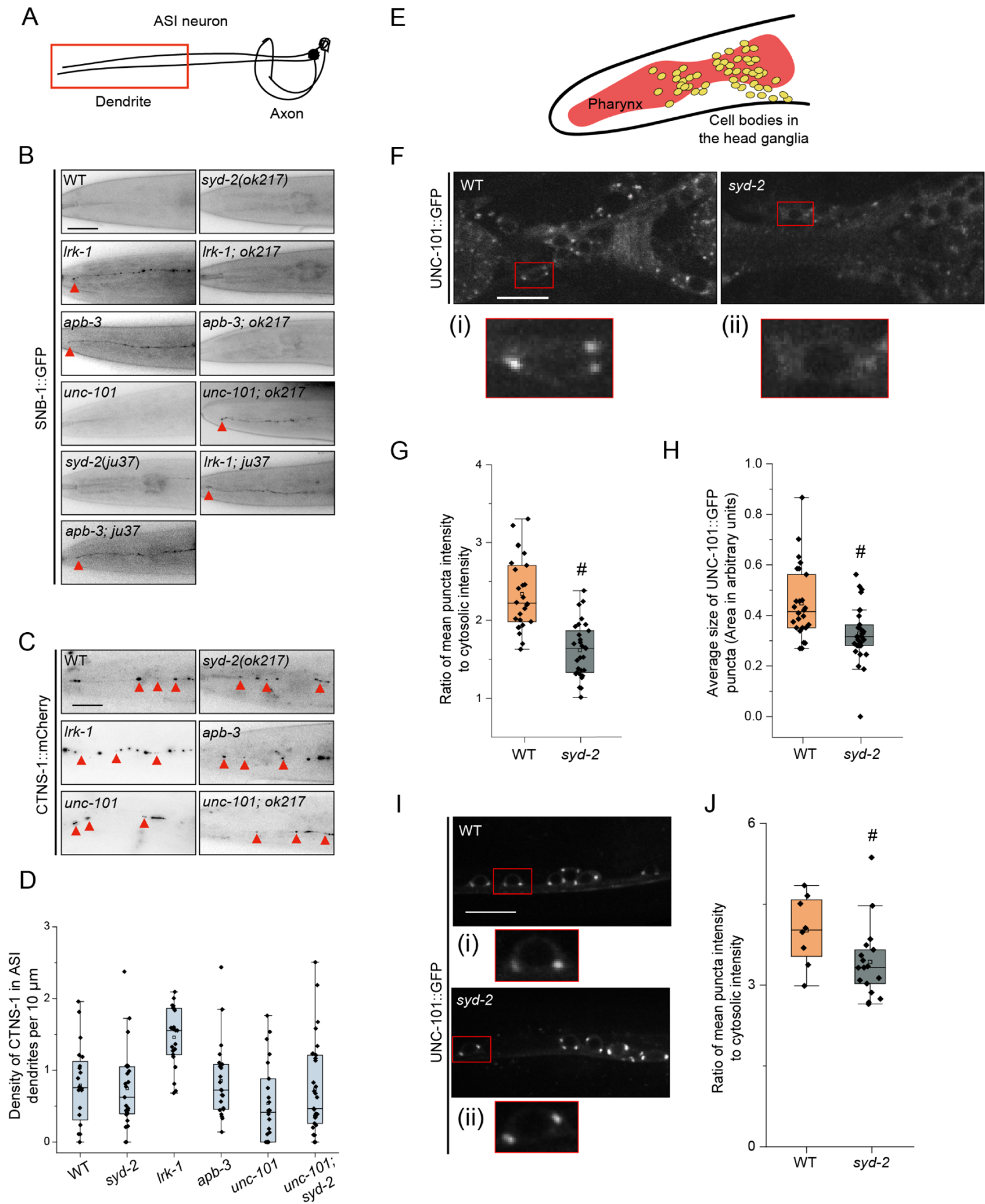
Figure 6
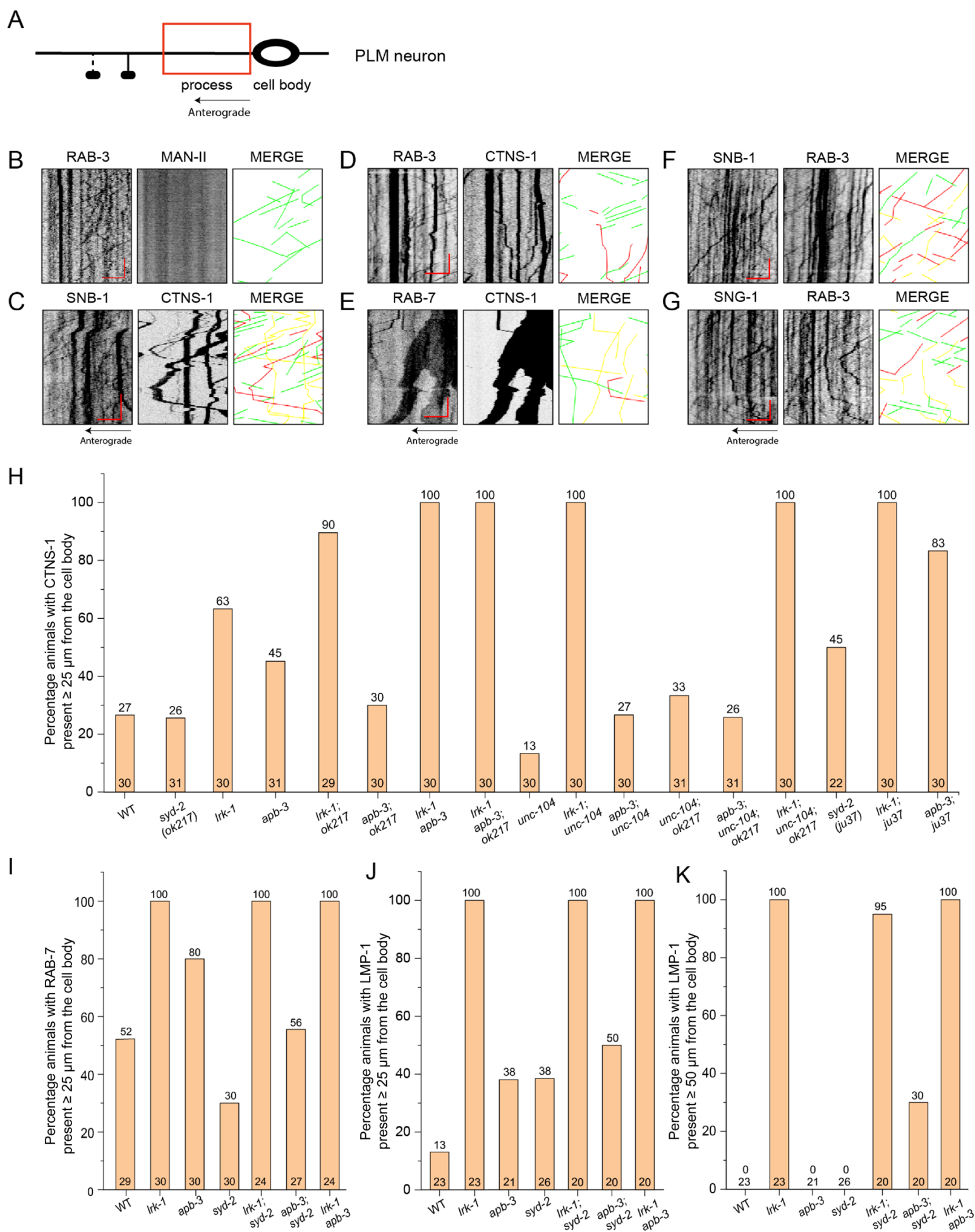
Supplementary Figure S1

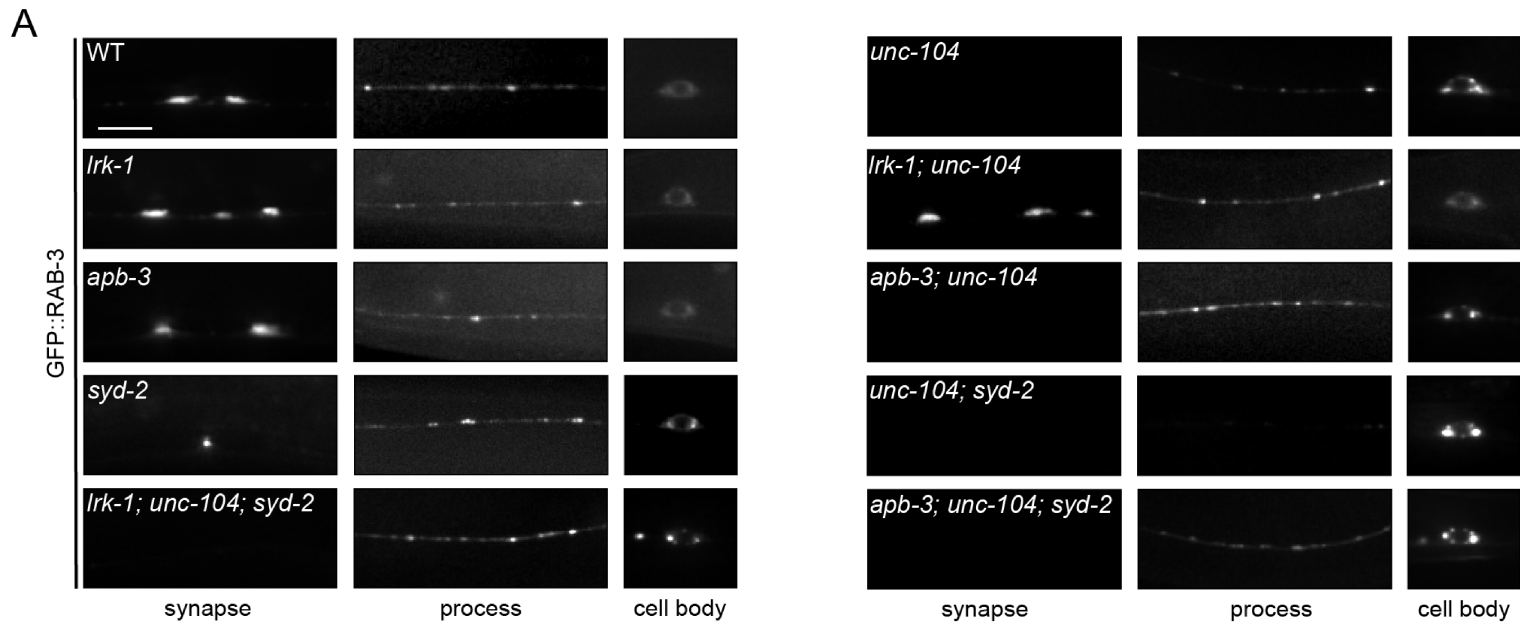**Supplementary Figure S2**

Supplementary Figure S3
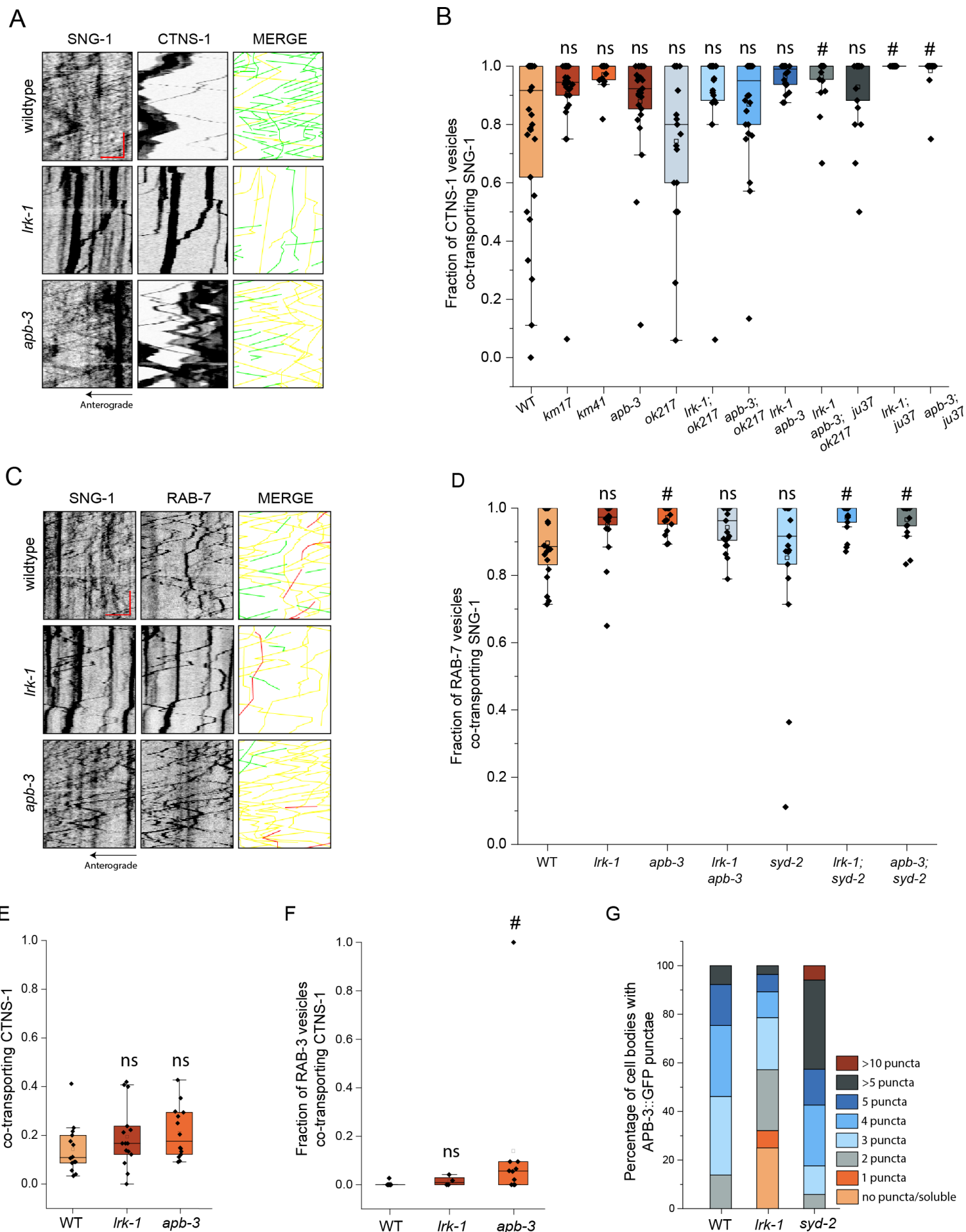
Supplementary Figure S4
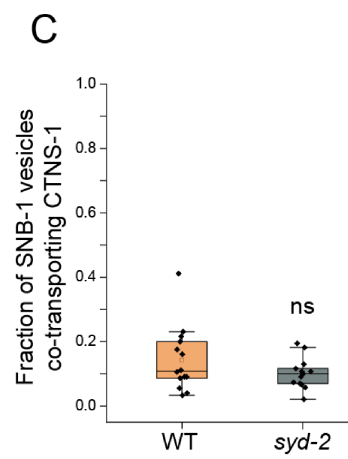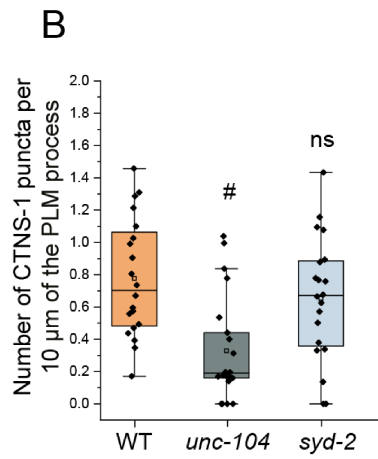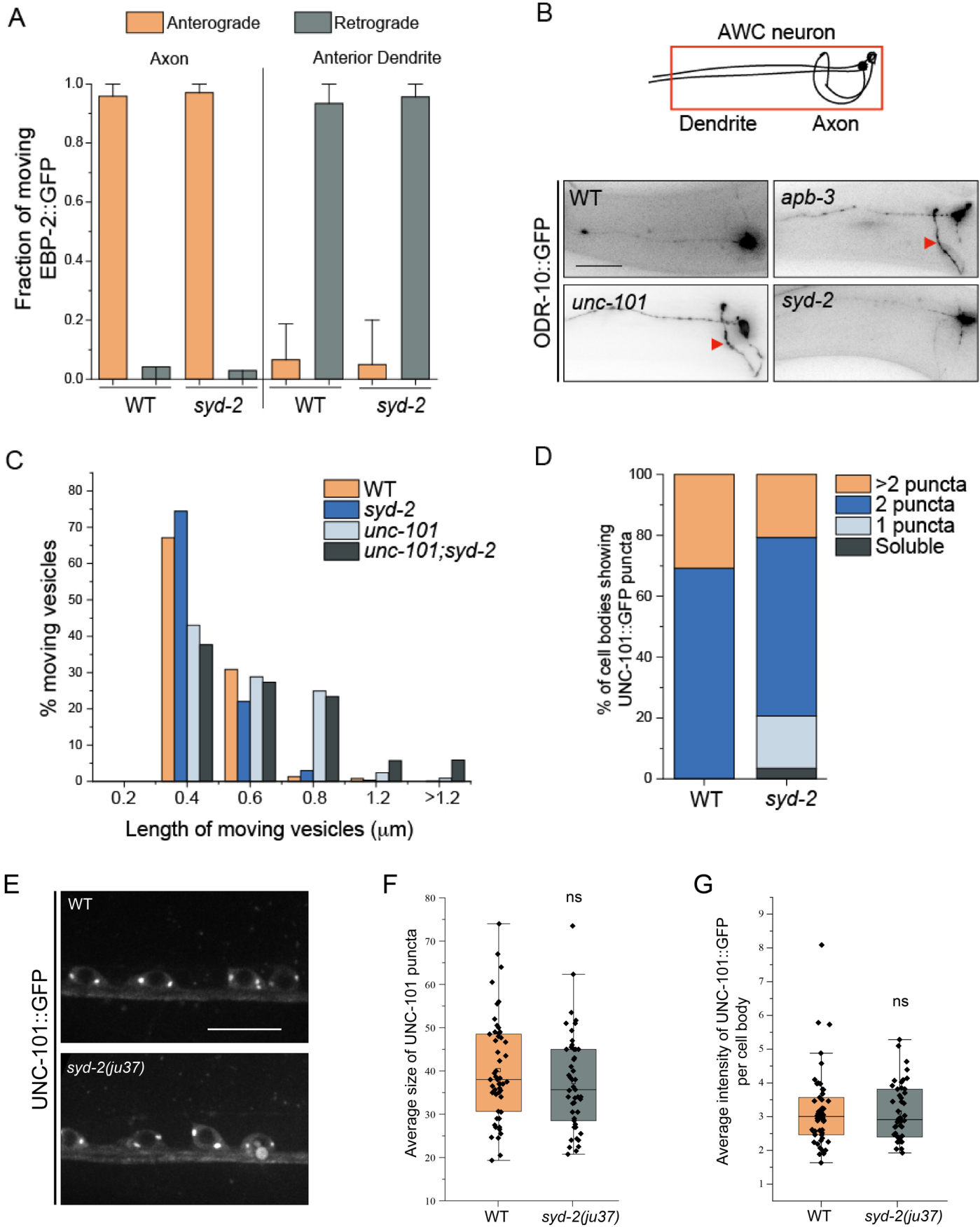
Table 1: SNB-1 in ASI

Genotype	Average % length of dendrite showing SNB-1 signal	Standard deviation
WT	39 %	27
lrk-1(km17)	92 %	2
apb-3(ok429)	69 %	28
syd-2(ok217)	25 %	25
lrk-1(km17); syd-2(ok217)	35 %	23
apb-3(ok429); syd-2(ok217)	45 %	28